Electron dynamics of a He atom in strong, oscillating magnetic fields

M. Sadhukhan*
Department of Chemical Sciences, Indian Institute of Science Education & Research, Mohanpur Campus, P. O. BCKV Main Campus, Mohanpur 741252, India

B. M. Deb†
Visva-Bharati University, Publishing Department, 6 A. J. C. Bose Road, Kolkata 700017, India
(Received 21 October 2013; published 30 April 2014)

The present numerical, time-dependent density-functional study of a He atom interacting with strong, oscillating magnetic fields shows that this scenario is quite different from the case of a laser electric field–He atom interaction. Signatures of sluggish electron dynamics are found in this study, while through a mechanical analogy the flow of electron density under such conditions has been explained. These calculations take into account both exchange and correlation. Through several calculated dynamical quantities, we have shown that, in contrast to the case of the (one-electron) H atom studied earlier, the nonlinear dependence of interelectronic repulsions (a combination of Coulomb, exchange and correlation terms) on the magnetic field plays a significant role in this strong-field electron dynamics in the He atom, which cannot be explained by a perturbative approach.

DOI: 10.1103/PhysRevA.89.042516 PACS number(s): 31.15.E−, 31.70.Hq, 32.10.−f

I. INTRODUCTION

The interaction between an atom or molecule and strong ($\approx 10^5$–10^8 T), static magnetic fields has been a subject of contemporary interest. These studies have been motivated by an urge to understand similar interactions between excitonic (electron-hole bound states) systems in semiconductors [1,2] for which the H atom is an atomic model. Later, astronomical discoveries of small atoms and molecules on the surfaces of extraterrestrial giant magnetic field sources (e.g., pulsars, white dwarfs, and neutron stars) have enhanced the relevance of such studies [3]. Among them He is the lightest many-electron system present. Therefore, the detailed electronic structure and dynamics of He atom under strong magnetic fields assumes considerable significance.

However, magnetic fields of such strengths cannot be achieved in terrestrial laboratories yet (the largest pulsed magnetic field achieved so far seems to be limited to 10^2 T [4]), thereby restricting the progress on this subject largely to theoretical studies. The interaction between such strong, static magnetic fields and the He atom has been studied extensively. These numerical studies span a wide spectrum of increasingly sophisticated techniques from Hartree-Fock [5,6], full configuration-interaction [7–9], and quantum Monte Carlo [10,11] to Kohn-Sham density-functional theory methods [12,13]. Such studies, most of which include accurate correlation effects, suggest an elongation of electron density in the direction of the applied strong magnetic field. It is also proposed that He atoms can make a long chain through this elongated electron density in the presence of such strong magnetic fields [12–15].

On the other hand, the interaction between a time-dependent (TD) magnetic field and the He atom (or any other many-electron atom or molecule) has not been explored yet. To our knowledge, there are only two recent works which deal with the dynamics [16] and quantum chaos [17] in H atom interacting with strong, oscillating magnetic fields. These studies reveal the existence of a considerably slower dynamics than that of the incident magnetic field, a resonance-energy-transfer phenomenon, and a nonlinear time evolution for the (one-electron) H atom. For a many-electron atom like the He atom, the situation is even more complicated due to the interelectronic repulsion. In contrast to this situation for strong, TD magnetic fields, its electrical counterpart, i.e., laser-atom and laser-molecule interactions have been dealt with extensively due to the routine availability of such intense lasers, in terrestrial laboratories. It has been shown by numerous theoretical studies including TD Hartree-Fock [18], quantum Monte Carlo [19], TD DFT [20,21] and pseudospectral methods [22] that the density interacting with an oscillating laser electric field moves back and forth, leading to a gradual oozing out through ionization channels. However, no such study appears to have been made so far for an oscillating, strong magnetic field interacting with two- and many-electron systems. However, as in the cases for laser fields, such strong-field interactions have to be treated nonperturbatively, because the perturbation here is not small compared to the unperturbed Hamiltonian.

The present work explores the electron dynamics of a He atom under strong, oscillating magnetic fields. For this purpose, the Deb-Chattaraj (DC) equation [23] has been extended to the strong, in general time-dependent, magnetic field regime using the quantum fluid dynamical route to TD DFT [24]. In this paper the real-time DC equation, involving both charge and current densities, will be solved numerically for He atom under strong, oscillating magnetic fields using an accurate numerical methodology developed in our laboratory [20,21,23,25].

The plan of the paper is the following: Sec. II briefly discusses the derivation of the DC equation followed by the computational methodology. Results will be discussed in Sec. III while Sec. IV summarizes the work.

*Present address: S. N. Bose National Centre for Basic Sciences, Block JD, Sector III, Salt Lake City, Kolkata 700098, India.
†Corresponding author: bmdeb@yahoo.co.in

II. FORMULATION

The TD Schrödinger equation for the He atom in a TD, arbitrarily strong, z-directional, spatially homogeneous magnetic field $\mathbf{B}(t)$ is given by (atomic units are employed throughout unless mentioned otherwise)

$$\left(-(1/2)\sum_k \{[\mathbf{p}_k - \mathbf{A}_k(t)/c]^2 - 1/r_k\} + 1/|\mathbf{r}_1 - \mathbf{r}_2|\right)\psi(\mathbf{r}_1,\mathbf{r}_2) = i\partial\mathbf{\Psi}(\mathbf{r}_1,\mathbf{r}_2)/\partial t, \quad (1)$$

where $\mathbf{p}_k = -i\nabla_k$ is the canonical momentum of the kth particle (in the present case, $k = 1,2$) and c is the speed of light. Under a symmetric gauge [15], the vector potential assumes the form

$$\mathbf{A}_k(\mathrm{t}) = [B(t)/2](y_k\mathbf{e}_x - x_k\mathbf{e}_y). \quad (2)$$

In order to satisfy the gauge condition, the two-particle wave function Ψ (normalized to unity) transforms as

$$\Psi \rightarrow \Psi\exp(i\lambda/c) \quad (3)$$

while the vector potential transforms as

$$\mathbf{A}_k(t) \rightarrow \mathbf{A}_k(t) + \nabla_k\lambda. \quad (4)$$

This problem of nonuniqueness associated with the phase of the wave function however does not exist in purely density-based quantities since the complex phase is "washed out" by the modulus operation to obtain the one-particle density:

$$\rho(\mathbf{r},t) = \int |\Psi(\mathbf{r},\mathbf{r}_2)|^2 d\mathbf{r}_2. \quad (5)$$

To obtain the electron density of the He atom directly, bypassing Eq. (5), we extend the QFDFT approach [23,24] (QF denotes Quantum Fluid) to include the presence of magnetic fields (with the formalism developed in Refs. [26,27]) as follows: The expectation value of the TD Hamiltonian in Eq. (1) is

$$\langle H\rangle(t) = \langle\Psi|H|\Psi\rangle, \quad (6)$$

which can be partitioned into two parts, viz., a field-free term E_0 and a magnetic term E_m. E_0 contains the electron-nuclear attraction energy, kinetic energy, and interelectronic repulsion terms, both classical and quantal in origin. The E_m term contains the effect of the TD magnetic field through the expression

$$E_m = (c^2/2)\langle\Psi|\sum_k A_k^2|\Psi\rangle - (i/2c)\langle\Psi|\sum_k \mathbf{A}_k\cdot\nabla_k|\Psi\rangle. \quad (7)$$

The first term on the right-hand side is a local operator and yields

$$\langle\Psi|\sum_k A_k^2|\Psi\rangle = [\beta^2(t)/2]\int \rho(r,t)(x^2+y^2)d\mathbf{r}, \quad (8)$$

where $\beta(t) = B(t)/B_0$; B_0 (not in atomic units) $= 2m^2e^3c/\hbar^3 = 4.7010 \times 10^5$ T, m and e being the mass and charge of the electron, respectively. The second term on the right-hand side of Eq. (7) vanishes identically under the assumption of cylindrical symmetry [27]. This assumption is equivalent to $\langle L_z\rangle = \langle\sum_k \mathbf{L}_z^k\rangle = 0$, where $\mathbf{L}_z^k$ is the z component of the orbital angular momentum of the kth electron. The above assumption can be justified in the following manner : Since the operator $\mathbf{A}_k\cdot\nabla_k$ is proportional to $\mathbf{B}\cdot\mathbf{L}_z^k$, i.e.,$\sum_k \mathbf{A}_k\cdot\nabla_k$ is proportional to $\mathbf{B}\cdot L_z(L_z = \sum_k \mathbf{L}_z^k)$, the operator $\boldsymbol{L}_z$ commutes with the Hamiltonian [Eq. (1)], provided $\mathbf{B}$ is not a function of space. Therefore, $\boldsymbol{L}_z$ turns out to be a constant of motion even for TD magnetic fields. Since the $t = 0$ state is the $^1S_0$ field-free ground state of the He atom, viz., $^1S_0$ where $\langle L_z\rangle = 0$, $\langle L_z\rangle$ will remain zero throughout the time evolution. Therefore, following the earlier work by Deb and Ghosh [24] the effective potential density for the electron fluid becomes

$$\int d\mathbf{r}h[\rho] = \int d\mathbf{r}\{G[\rho] + \frac{1}{2}\int \rho(\mathbf{r}',t)\rho(\mathbf{r},t)/(|\mathbf{r}-\mathbf{r}'|)d\mathbf{r}' + V_{\mathrm{ext}}(\mathbf{r})\rho(\mathbf{r},t) + [\beta^2(t)/2]\rho(\mathbf{r},t)(x^2+y^2)\}, \quad (9)$$

where $V_{\mathrm{ext}}(\mathbf{r})$ is the external potential and $G[\rho]$ includes exchange and correlation terms. Hence, a strong magnetic field introduces only an additive term in the potential. Following the variational path created by the addition of the resultant Navier-Stokes and continuity equations, we obtain the final DC equation for the He atom in strong, TD magnetic fields as

$$[-(1/2)\nabla^2 + V_{\mathrm{eff}}]\Phi(\mathbf{r},t) = i\partial\Phi(\mathbf{r},t)/\partial t, \quad (10)$$

where the effective potential

$$V_{\mathrm{eff}}(\mathbf{r},t) = V_{\mathrm{att}}(\mathbf{r},t) + V_{e\text{-}e}(\mathbf{r},t) + V_x(\mathbf{r},t) + V_{\mathrm{corr}}(\mathbf{r},t) + V_m(\mathbf{r},t) + \delta T_{\mathrm{corr}}/\delta\rho \quad (11)$$

and the complex-valued hydrodynamical function $\Phi(\mathbf{r},t)$ generates the TD normalized electron density

$$\rho(\mathbf{r},t) = |\Phi(\mathbf{r},t)|^2, \quad (12)$$

$$\int \rho(\mathbf{r},t)d\mathbf{r} = 2. \quad (13)$$

In Eq. (11), the attraction potential $V_{\mathrm{att}}(\mathbf{r},t) = -2/\mathbf{r}$, the Coulomb repulsion $V_{e-e}(\mathbf{r},t) = \int \rho(\mathbf{r}',t)/(|\mathbf{r}-\mathbf{r}'|)d\mathbf{r}'$ and the magnetic potential $V_m(\mathbf{r},t) = [\beta^2(t)/2]\rho(\mathbf{r},t)(x^2+y^2)$ are classical terms whereas the exchange potential $V_x(\mathbf{r},t)$ and the correlation potential $V_{\mathrm{corr}}(\mathbf{r},t)$ are purely quantum in origin. The last term of Eq. (11) is the kinetic-energy correction term added to the Weizsäcker kinetic energy. For two-electron systems, T_{corr} is negligible and vanishes identically for a Hartree-Fock wave function. Although we include electron correlation in the present work, we neglect T_{corr} because for the He atom the correlated density is locally quite close to the Hartree-Fock density. Note that so far no approximate, though accurate, universal functional for T_{corr} has been found. Once found, the long-prevailing kinetic-energy problem [28] will be solved, leading to a drastic simplification of the electronic structure calculations of N-electron systems through a single DC equation, instead of solving N coupled equations as in any other method. Although the contribution from T_{corr} to the total energy has been shown to be positive, we assume that due to its smallness no qualitative change would occur in our conclusions even if it were included.

In the present work, we have used the exact exchange functional [29]

$$V_x(\mathbf{r},t) = (-1/2)\int \rho(\mathbf{r}',t)/(|\mathbf{r}-\mathbf{r}'|)d\mathbf{r}' \quad (14)$$

while a parametrized Wigner correlation functional is used. It is known that the Wigner correlation functional

$$V_{\rm corr}(\mathbf{r},t) = \delta E_{\rm corr}/\delta\rho = -[a + c\rho(\mathbf{r},t)^{-1/3}]/[a + b\rho(\mathbf{r},t)^{-1/3}]^2, \quad (15)$$

where $a = 9.81$, $b = 21.437$, and $c = (4/3)b = 28.582\,667$, provides a very good estimate of correlation energies for various atoms and molecules [25,27,29,30], in both ground and excited states, due to the correct local and global behavior of the functional as well as its functional derivative. The quantity $E_{\rm corr}(t)$ given by

$$E_{\rm corr}(t) = -\int \rho(\mathbf{r},t)/[a + b\rho(\mathbf{r},t)^{-1/3}]d\mathbf{r} \quad (16)$$

is used as the TD correlation "energy." Note that the one-to-one correspondence between the charge density and the external potential is strictly applicable only for the ground state. The current density $\mathbf{j}(\mathbf{r},t)$ is also required to uniquely determine any other stationary state. It is also shown that both E_x and $E_{\rm corr}$ depend on $\mathbf{j}(\mathbf{r}, \mathrm{t})$ in the presence of magnetic fields [26]. Although the functional forms of E_x and $E_{\rm corr}$ have been formulated for a static electron density, we phenomenologically translate the same forms to dynamical cases incorporating the time dependence implicitly through $\rho(\mathbf{r},t)$ which contains information, in principle, about all stationary states.

The scaled magnetic field $\beta(t)$ is chosen as

$$\beta(t) = \beta_{\rm max} f(t)\sin(\omega_B t), \quad (17)$$

where the ramp function $f(t)$ is

$$f(t) = \begin{cases} t/t_0 & \text{if } t < t_0, \\ 1 & \text{if } t \geqslant t_0, \end{cases} \quad (18)$$

t_0 being the time to complete five magnetic cycles. This linear ramp function has been introduced to avoid a sudden shock to the electron density from the external field which, even in true experimental conditions, takes a finite time to reach its peak value. Note also that a free electron would rotate in a circular orbit with radius equal to the innermost Bohr radius (a_0) for the peak value of the magnetic field, i.e., $\beta_{\rm max} = 0.5$ [15]. It can be seen from the form of V_m that, due to its sine-squared dependence on ω_B, V_m has a frequency $2\omega_B$, i.e., $2\sin^2(\omega_B t) = 1 - \cos(2\omega_B t)$.

To solve Eq. (10) numerically, we follow the Alternating Direction Implicit (ADI) scheme [23,25] in cylindrical coordinates ($0 \leqslant \tilde{\rho} \leqslant \infty$, $-\infty \leqslant \tilde{z} \leqslant +\infty$, $0 \leqslant \varphi \leqslant 2\pi$), the magnetic field being applied along $\tilde{z}$, i.e., the axis of the cylinder. The space grid has been discretized as follows:

$$\tilde{\rho} = \mathrm{x}^2,$$
$$x_i = \delta + ih, \quad \delta = 1 \times 10^{-6}, \quad \mathrm{i} = 1,2,\ldots,N_1,$$
$$\tilde{z}_k = [-(N_2 - 1)/2 + k]h, \quad \mathrm{k} = 1,2,\ldots,N_2,$$
$$h = 0.02\,\text{a.u.}, \quad \Delta t = 0.002\,\text{a.u.}, \quad \mathrm{N}_1 = 121, \quad \mathrm{N}_2 = 501.$$

Due to cylindrical symmetry, φ has been integrated out. Each magnetic cycle contains 4096 time steps while the magnetic field frequency $\omega_B = 2\pi/(4096\Delta t) = 0.767$ a.u. We have followed the dynamics for 50 magnetic cycles, i.e., 409.6 a.u. or 9.9082 fs (1 a.u. = 0.024 19 fs), covering 204 830 time steps. Important physical features of the interaction develop by this time. The calculations were launched by taking the Hartree-Fock ground-state density from Ref. [31] as the initial ($t = 0$) density. Nevertheless, since we have incorporated electron correlation in our TD DC equation, the results incorporate the correlation effects by the end of the ramp and continue up to the end of the 50th cycle. Because of the large number of time steps involved in this computation, the internal consistency of the results has been thoroughly checked.

III. RESULTS AND DISCUSSION

In this section, we will interpret in detail the features of the electron density in the He atom under the influence of strong, oscillating magnetic fields. In particular, differences from the H atom due to the presence of another electron will be highlighted.

We start by calculating the average distance in the $\tilde{\rho}$ direction [$\langle\tilde{\rho}\rangle(t)$] of the electron density,

$$\langle\tilde{\rho}\rangle(t) = \int \tilde{\rho}\rho(\mathbf{r},t)d\mathbf{r}, \quad (19)$$

for $\beta_{\rm max} = 0.2$, 0.4, 0.6, 0.8, and 1.0 (Fig. 1). For $\beta_{\rm max} = 0.2$ and 0.4, short- and long-time-period components of the oscillations in $\langle\tilde{\rho}\rangle(t)$ are detected. Both these time periods, however, are larger than the incident magnetic field time period; the time period of the faster component $\approx$10.24 a.u. or 0.255 fs. Note that the electron density does not respond to the two halves of a magnetic cycle (in a magnetic cycle, the magnetic potential reaches its peak value twice) separately for $\beta_{\rm max} = 0.2$. When the field strength increases to $\beta_{\rm max} = 0.4$, the density starts responding to the two halves separately, leading to prominent bifurcations in the fast oscillations. For $\beta_{\rm max} = 0.6$, the $\langle\tilde{\rho}\rangle(t)$ decreases initially but attains an almost steady mean value at the end of the ramp (five magnetic cycles) around which the fast oscillations occur. The bifurcations of the peaks are now more prominent. At this field strength, therefore, the density *contracts* significantly in the $\tilde{\rho}$ direction (perpendicular to the magnetic field) and responds individually to each of the two halves of a magnetic cycle. For $\beta_{\rm max} = 0.8$ and 1.0, significant increase in $\langle\tilde{\rho}\rangle(t)$ occurs after the ramp, indicating an *expansion* of density along the $\tilde{\rho}$ direction.

In order to explain these results we invoke interelectronic repulsion, which results from a combination of Coulomb, exchange, and correlation terms. Consider the zero-field electron density as a spherical "ball of jelly" at $t = 0$. When a nonzero magnetic field is applied along the $\tilde{z}$ direction the oscillating magnetic potential

$$V_m(\mathbf{r},t) = [\beta^2(t)/2]\tilde{\rho}^2 \quad (20)$$

"pressurizes" the electron density along the $\tilde{\rho}$ direction. As a result of this oscillating "squeezing" potential the interelectronic repulsion also varies periodically, resisting further density contraction. The "force" due to V_m,

$$\mathbf{F}_m = -\beta^2(t)\tilde{\boldsymbol{\rho}}, \quad (21)$$

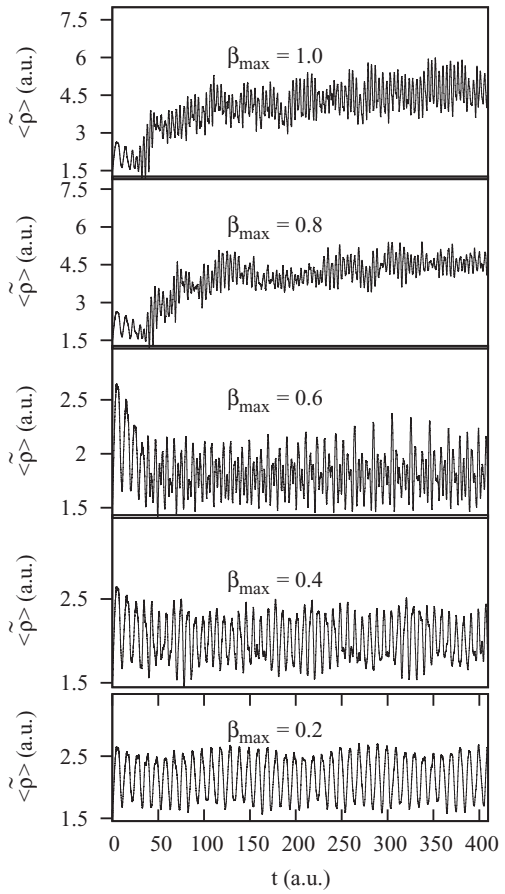

FIG. 1. The time evolution of $\langle\tilde{\rho}\rangle(t)$ for $\beta_{max} = 0.2$, 0.4, 0.6, 0.8, and 1.0 from the bottom to the top. Note the change of appearance for $\beta_{max} \geqslant 0.6$ which signifies a distinct change in dynamics, i.e., from elastic to plastic flow (atomic units).

moves a fictitious particle of unit mass always towards the nucleus (since $\mathbf{F}_m \leqslant 0$; for all t) with acceleration

$$\mathbf{a}(\mathbf{r},t) = -[\beta^2(t)]\tilde{\boldsymbol{\rho}}. \tag{22}$$

However, even when the magnetic field (hence, the acceleration) vanishes in the middle or at the end of a magnetic cycle, the particle is allowed to move with a constant "velocity" $\mathbf{v}$ such that

$$d\mathbf{v}/d\mathrm{t} = \mathbf{F}_m = 0. \tag{23}$$

Therefore the motion of electron density is sustained even when the magnetic field temporarily vanishes until the increased interelectronic repulsion forces the density to expand again. This expansion continues until the magnetic "force" overrides the decreased interelectronic repulsion again. For this reason the electron density follows a slow dynamics under strong, oscillating magnetic fields. Note that the acceleration due to a $\tilde{z}$-directional laser electric field is

$$\mathbf{a}_L = E_0 \sin(\omega_L t)\mathbf{e}_z, \tag{24}$$

where E_0, ω_L, and $\mathbf{e}_z$ represent the peak electric field, laser frequency, and unit vector in the $\tilde{z}$ direction, respectively. Since the acceleration changes sign for this case the direction of $\mathbf{v}$ also alters twice in an optical cycle. As a result, when the laser electric field vanishes the electron density halts momentarily at a $\tilde{z}$-symmetric configuration.

Next we examine the density [Fig. 2(a)] and the difference density [Fig. 2(b)]

$$\Delta\rho(\mathbf{r},t;\beta_{max}) = \rho(\mathbf{r},t;\beta_{max}) - \rho(\mathbf{r};\beta_{max} = 0) \tag{25}$$

to elucidate the density reorientation in further detail. Positive and negative $\Delta\rho$ values signify density accumulation and depletion, respectively, separated by the zero $\Delta\rho$ lines, in different regions of space, thereby giving a detailed picture of the TD charge reorganization as a result of the interaction. The present results are obtained at the end of the 30th magnetic cycle (i.e., when the field vanishes). Since no significant visual change has been detected for $\beta_{max} = 0.2$, we report only the results for $\beta_{max} = 0.4$, 0.6, 0.8, and 1.0. For $\beta_{max} = 0.4$, the density is accumulated in the $\tilde{\rho}$ direction as well as in the $\tilde{z}$ direction. A prominent density depletion is also observed near the nucleus along the $\tilde{\rho}$ direction. At $t = 0$, the electron density falls exponentially from the nuclear site. Therefore when the magnetic field tries to pull more electron density towards the nucleus, the interelectronic repulsion increases largely near the nucleus. This process finally leads to a density depletion from this region in order to decrease the interelectronic repulsion. As the field strength increases to $\beta_{max} = 0.6$, the density expands more in the $\tilde{z}$ direction compared to the $\tilde{\rho}$ direction which explains the decrease in the $\langle\tilde{\rho}\rangle(t)$ profile at this magnetic field. For $\beta_{max} = 0.8$ and 1.0, the density again expands along the $\tilde{\rho}$ direction. Additionally, an increase in the size of the negative $\Delta\rho$ region near the nucleus for each of these two cases is observed, which indicates an increased interelectronic repulsion for $\beta_{max} = 0.8$ and 1.0.

However, we negate the possibility of density reflections from the grid boundaries which cause unphysical effects in density reorientation through the following arguments: First, the density at the grid boundaries drops significantly to at most 10^{-5} for all the cases reported here. Second, during computation at each time step, the non-normalized electron density, when integrated over space, deviates from 2 only by a small amount, which retains the same order of magnitude throughout the time evolution (e.g., for $\beta_{max} = 1.0$, this deviation is $\pm 10^{-4}$ throughout the time evolution). Had the density been reflected from the grid boundaries it would increase significantly after reflection. Note that such reflections cause a serious problem in studying the interactions between intense laser fields and atoms or molecules.

The above discussions require an investigation of the interelectronic interaction as a function of time. However, due to the inevitable energy-time uncertainty relation in quantum mechanics, "energy" is not an observable in any dynamical situation, including the present case. Nevertheless, one can invoke the notion of TD quasienergy as a measure of interelectronic interaction considering a time step as a fictitious "snapshot" of the dynamics, while it should be borne into mind that these quantities are of only formal use. Thus, we use the TD expectation value of the Coulomb repulsion potential as repulsion "energy," viz.,

$$E_{rep}(t) = (1/2)\int V_{e\text{-}e}(\mathbf{r})\rho(\mathbf{r},t)d\mathbf{r}, \tag{26}$$

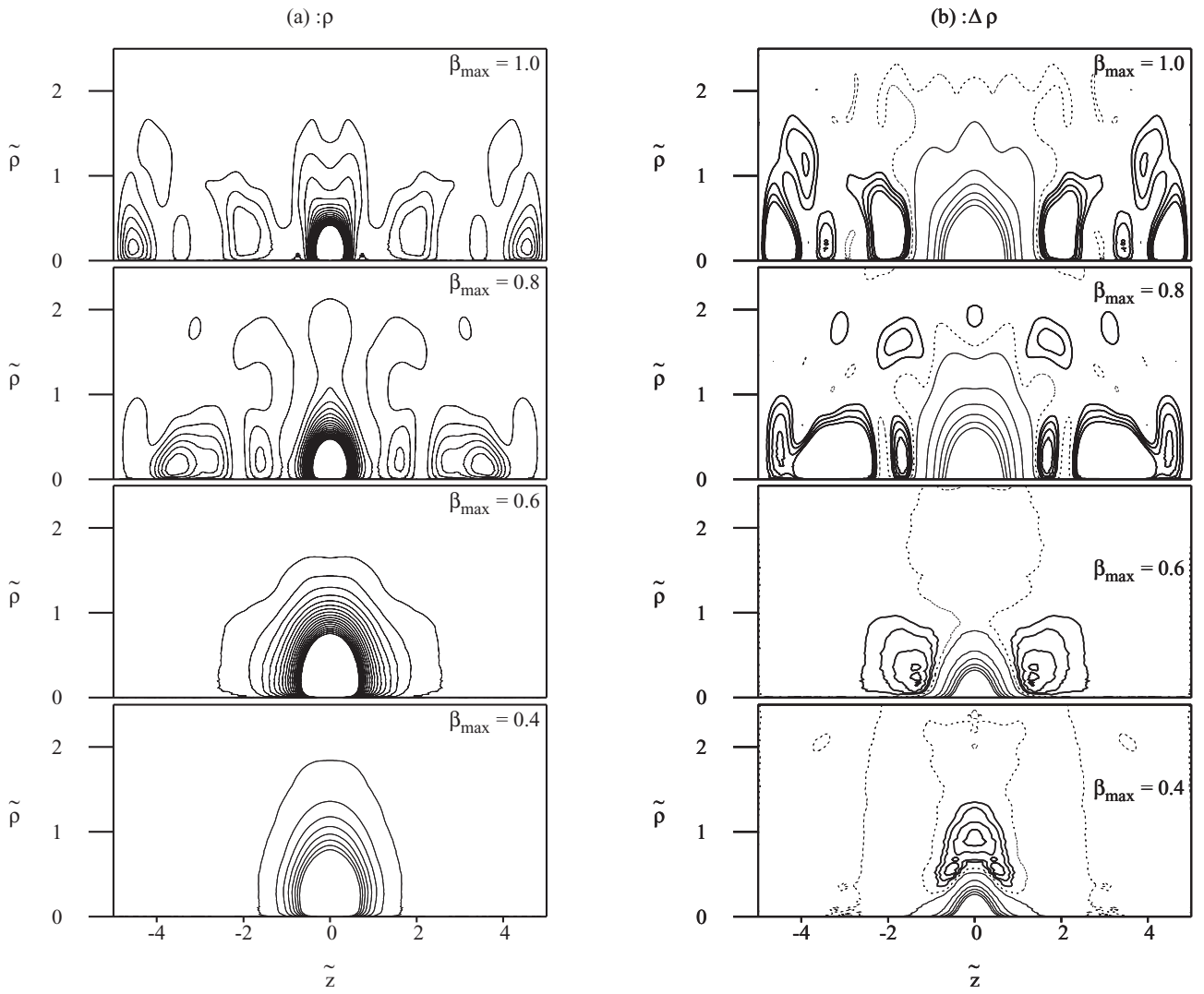

FIG. 2. (a) The electron density ρ, and (b) the corresponding difference density $\Delta\rho$ plots for $\beta_{max} = 0.4$, 0.6, 0.8, and 1.0. For density plots, the outer and inner contours correspond to $\rho = 0.008$ and 0.22, respectively. For $\Delta\rho > 0$, marked as thick solid lines, the contour values are 0.007, 0.01, 0.014, and 0.018. For $\Delta\rho < 0$, marked by thin solid lines, the outer and inner contour lines represent -0.01 and - 0.26 density values, respectively. The dotted lines are for $\Delta\rho = 0$ (atomic units).

which is expected to play an important role in the dynamics. These results for $\beta_{max} = 0.2$, 0.4, and 0.6 are presented in Fig. 3. For $\beta_{max} = 0.2$, the profile follows a similar structure to that presented in Fig. 1 for $\langle\tilde{\rho}\rangle(t)$ at this magnetic field. This feature indicates that as the electron density tries to come back to its original state, the repulsion "energy" increases and subsequently decreases once the electron density moves away from its original configuration, leading to the periodic temporal variations. Clearly, at lower magnetic fields one of the major contributors to the electron dynamics is the interelectronic repulsion. This conclusion is supported by the TD repulsion "energy" plot for $\beta_{max} = 0.4$, where it follows the same pattern as for $\beta_{max} = 0.2$. Supporting the above conclusion, the $E_{rep}(t)$ plot for $\beta_{max} = 0.6$ shows an oscillating rise, which is justified from the fact that at this magnetic field the electron density experiences a pressure which deforms its shape (Fig. 3) significantly but still tries to retain its original structure. Therefore, one can identify this magnetic field as a *threshold field* where the repulsion has reached such a high value that with slightly higher pressure the electron density will "flow away" from its ground state structure like a "plastic" material. Indeed, the cases for $\beta_{max} = 0.8$ and 1.0 (Fig. 4) support such a plastic flow. The buildup of the interelectronic repulsion during the ramp is evident for both cases. On the other hand, the consequent decay to a lower repulsion "energy" occurs through the spreading of density along the $\tilde{z}$ direction, thereby decreasing interelectronic repulsions. Although for both these magnetic fields the repulsion "energy" profile looks similar, one notices that for $\beta_{max} = 0.8$ the electron density reaches its maximum around the end of the magnetic cycle while for $\beta_{max} = 1.0$ it attains the same earlier and the decay starts even before the ramp ends at $t = 40.96$ a.u. This feature arises from the fact that for higher magnetic field the "elastic limit" for the density is attained earlier due to increased pressure. Therefore, there is a possibility that an "elastic threshold" does exist for the electron dynamics.

Since the present method also incorporates electron correlation effects, apart from Coulomb and exchange interactions,

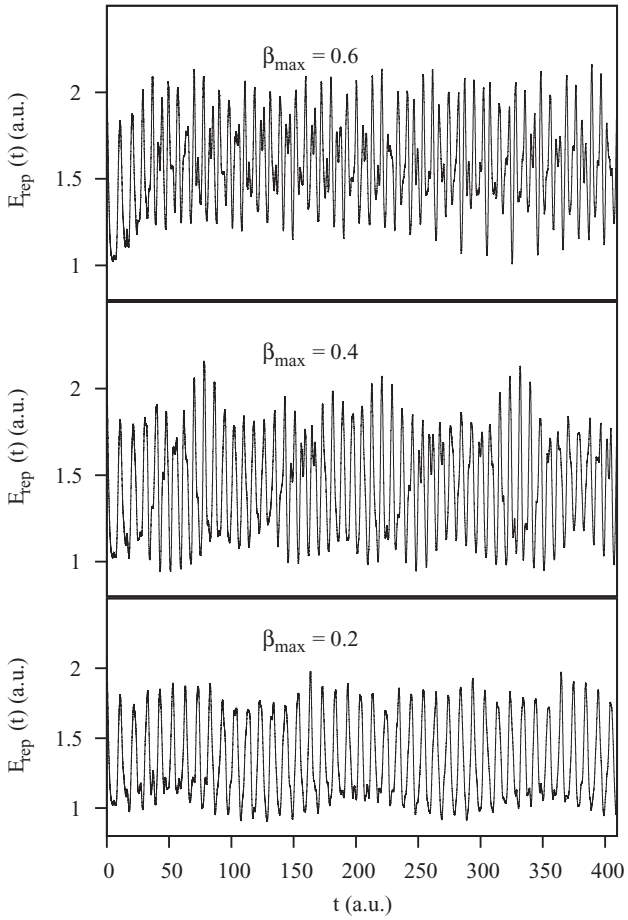

FIG. 3. TD interelectronic repulsion energies (a.u.) for $\beta_{\max} =$ 0.2, 0.4, and 0.6. The repulsions increase for a particular magnetic field strength due to the "pressure" by magnetic fields.

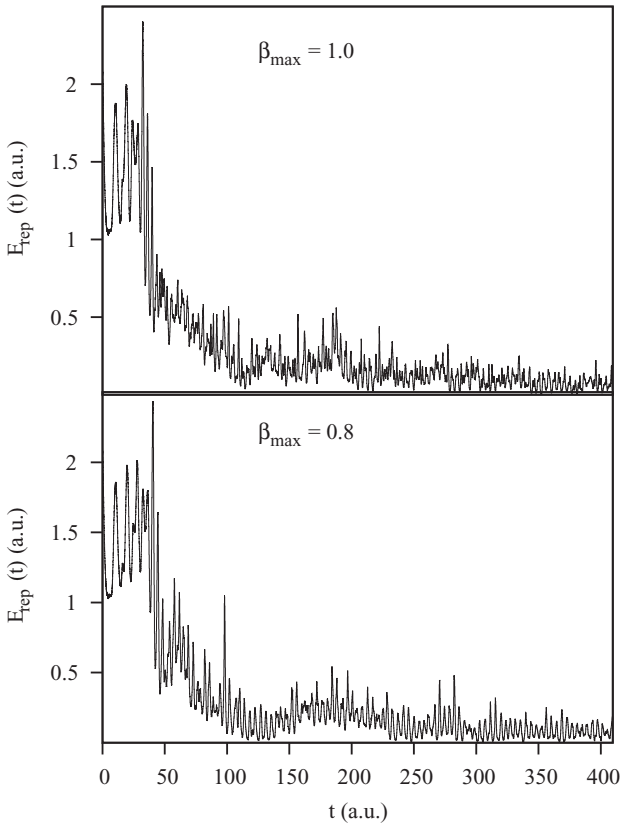

FIG. 4. TD interelectronic repulsion energies (a.u.) for $\beta_{\max} =$ 0.8 and 1.0. The sharp decrease signifies a relaxed response due to density spreading.

as a part of interelectronic repulsion, one can calculate the TD correlation "energy" $E_{\rm corr}(t)$ in the same spirit as the Coulomb repulsion and kinetic "energies" mentioned above; this is defined in Eq. (16) of the previous section. Since we have used exact exchange for the He atom in the present calculations—numerically half of the Coulomb repulsion—these results along with $E_{\rm rep}(t)$ encompass all the interelectronic effects in He atom dynamics in the present study. Figure 5 depicts $E_{\rm corr}(t)$ for $\beta_{\max} = 0.2$, 0.4, and 0.6. One can conclude from these results that electron correlation does not change drastically until $\beta_{\max} = 0.6$ although an increasing sensitivity to the magnetic fields with the increase of magnetic field strengths is apparent. This implies that up to $\beta_{\max} = 0.6$, the electronic configuration of He does not vary much with the increase in field strength, indicating that highly excited states of He have not been reached. Since all the doubly excited states of He are autoionizing [21] because of interelectronic repulsions, this situation means that through its spread in the $\tilde{z}$ direction, the electron density does not ooze out until $\beta_{\max} = 0.6$. To check this conclusion for higher magnetic fields, we calculated $E_{\rm corr}(t)$ for $\beta_{\max} = 0.8$ and 1.0. From these results (Fig. 6), one can see that the correlation effects actually decrease as the density begins its "plastic flow" along the $\tilde{z}$ direction at $\beta_{\max} = 0.8$, indicating diminished interelectronic repulsions. However, note that, although diminished, the value of $E_{\rm corr}(t)$ remains high enough to warrant a beyond-Hartree-Fock type of description in such cases.

To get a better insight into the details of the dynamics we have recorded the density values seen by six space-fixed observers, viz., A, B, C, D, E, and F corresponding to space points (3.0276,0), (1,0), (3.0276,3), (3.0276,−3), (1,3), and (1,−3), respectively, where the values in parentheses denote the $(\tilde{\rho},\tilde{z})$ coordinates of the points. These space points are chosen such that density fluctuations over space, with changes in magnetic field strengths, can be depicted graphically. On the other hand, since the values of C and D or E and F are identical due to the $\tilde{z}$ parity of the system, proving a numerical check on our computations, we will present only the results of points A, B, C, and E for $\beta_{\max} = 0.4$, 0.6, 0.8, and 1.0. Due to their relative insignificance in the interpretive process, the results for $\beta_{\max} = 0.2$ are not presented here. The time-dependent density fluctuations as seen by observer A, i.e., $\rho_{\rm A}(t)$, for four magnetic fields are presented in Fig. 7. It is seen that as the magnetic field strength increases from $\beta_{\max} = 0.2$ to 0.4, the density contracts along the $\tilde{z}$ direction but as $\beta_{\max}$ reaches 0.8 a significant amount of density builds up at the A point. For $\beta_{\max} = 1.0$, this effect is even more significant. This may appear counterintuitive but, as explained in the context of Fig. 2, the increased electron repulsion due to the magnetic

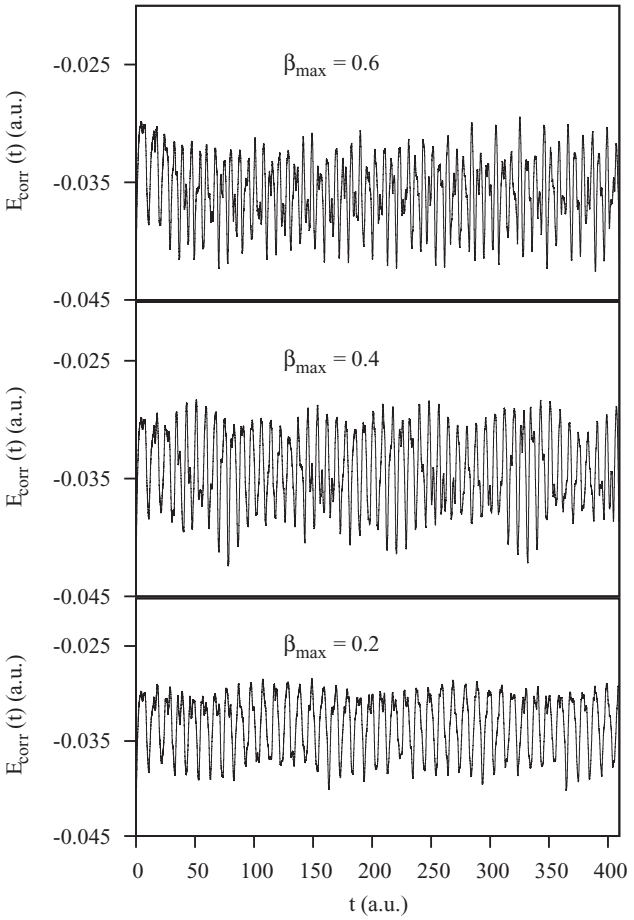

FIG. 5. TD correlation "energies" (a.u.) for $\beta_{max} = 0.2$, 0.4, and 0.6. Note the smallness of the overall change with increasing magnetic fields.

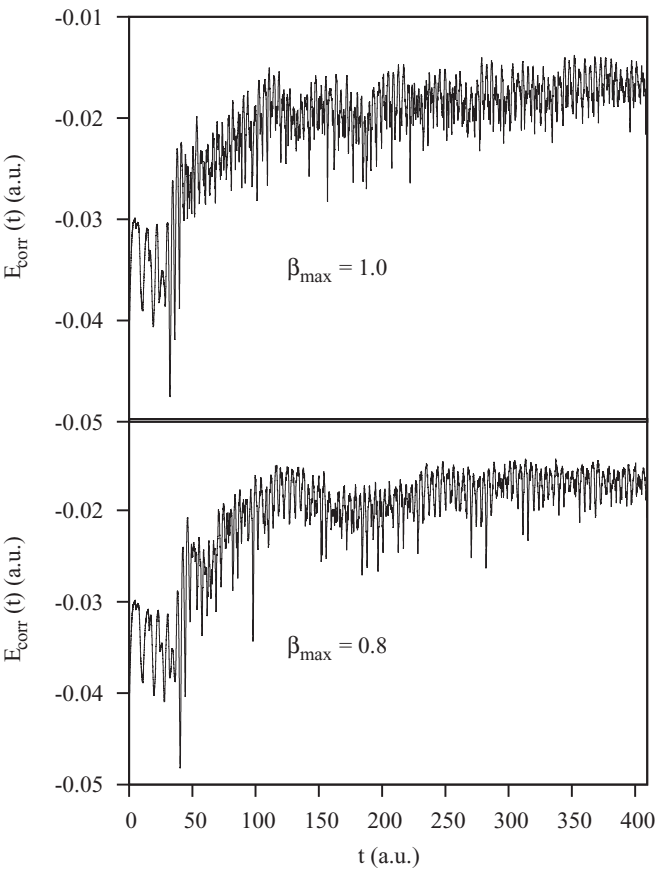

FIG. 6. $E_{corr}(t)$ values (a.u.) for $\beta_{max} = 0.8$ and 1.0. Note that although the value decreases as the density spreads, it does not become negligible in either case.

fields actually accumulates a significant amount of electron density along the $\tilde{\rho}$ direction.

From Fig. 2 one realizes that this density buildup happens at the cost of a density depletion near the nucleus along the $\tilde{\rho}$ direction. Figure 8 depicts the TD density fluctuations as observed by observer B. These reveal that while for $\beta_{max} = 0.4$ and 0.6 the overall densities do not change significantly at B, for $\beta_{max} = 0.8$ a sharp decay after the ramp indicates a rapid density depletion at B. The same conclusion can also be drawn for $\beta_{max} = 1.0$. Moreover, a little rise in density at B followed by a fall for $\beta_{max} = 0.8$ reveals a competition between the effects caused by the electron-nuclear attraction and the TD magnetic field. Although initially dominated by the TD magnetic field, after some time it again tries to return to its original form which of course is transient. Therefore, as expected, when the magnetic dominance is increased via the increased magnetic field strength ($\beta_{max} = 1.0$), the density can no longer be dominated by nuclear attraction, and interelectronic repulsions begin to play a significant role in the overall phenomenon.

However, for the observer C, depicted in Fig. 9, the density is swept away as the magnetic field increases from $\beta_{max} = 0.4$ to 0.6 which is a consequence of magnetic pressure along the $\tilde{\rho}$ direction. But, when the magnetic field increases further to $\beta_{max} = 0.8$, the density again flows back to this point. On the contrary, for an even stronger magnetic field $\beta_{max} = 1.0$, the density again contracts along the $\tilde{\rho}$ direction. This behavior is a consequence of the fact that for $\beta_{max} = 0.8$ the density that has been squeezed and has escaped from Coulomb attraction experiences too much interelectronic repulsion to be stable and therefore, as a trade-off, it tries to accommodate itself along the $\tilde{\rho}$ direction but away from the nucleus, which in turn diminishes the interelectronic repulsion. But, for $\beta_{max} = 1.0$, due to the increased magnetic pressure along the $\tilde{\rho}$ direction, that opportunity does not arise. Note that for all the four β_{max} values in Fig. 9, density does not decrease at all; rather, it increases significantly for $\beta_{max} = 0.8$ and 1.0. Therefore, it appears that the increased density at C also comes from the region near the nucleus where the observer B is stationed.

Figure 10 depicts the density fluctuations as experienced by observer E. For $\beta_{max} = 0.4$, 0.6, and 0.8, the electron density increases when the magnetic field increases, while for $\beta_{max} = 1.0$ the density does not increase at E compared to the situation for $\beta_{max} = 0.8$. On the contrary, a slight decrease in density is observed for $\beta_{max} = 1.0$. Therefore, this figure indicates an initial $\tilde{z}$ movement of density due to the increased pressure of the magnetic field. However, supporting our previous conclusion, the density begins a significant movement along the $\tilde{\rho}$ direction until it again experiences the magnetic pressure, leading to the results of Fig. 10.

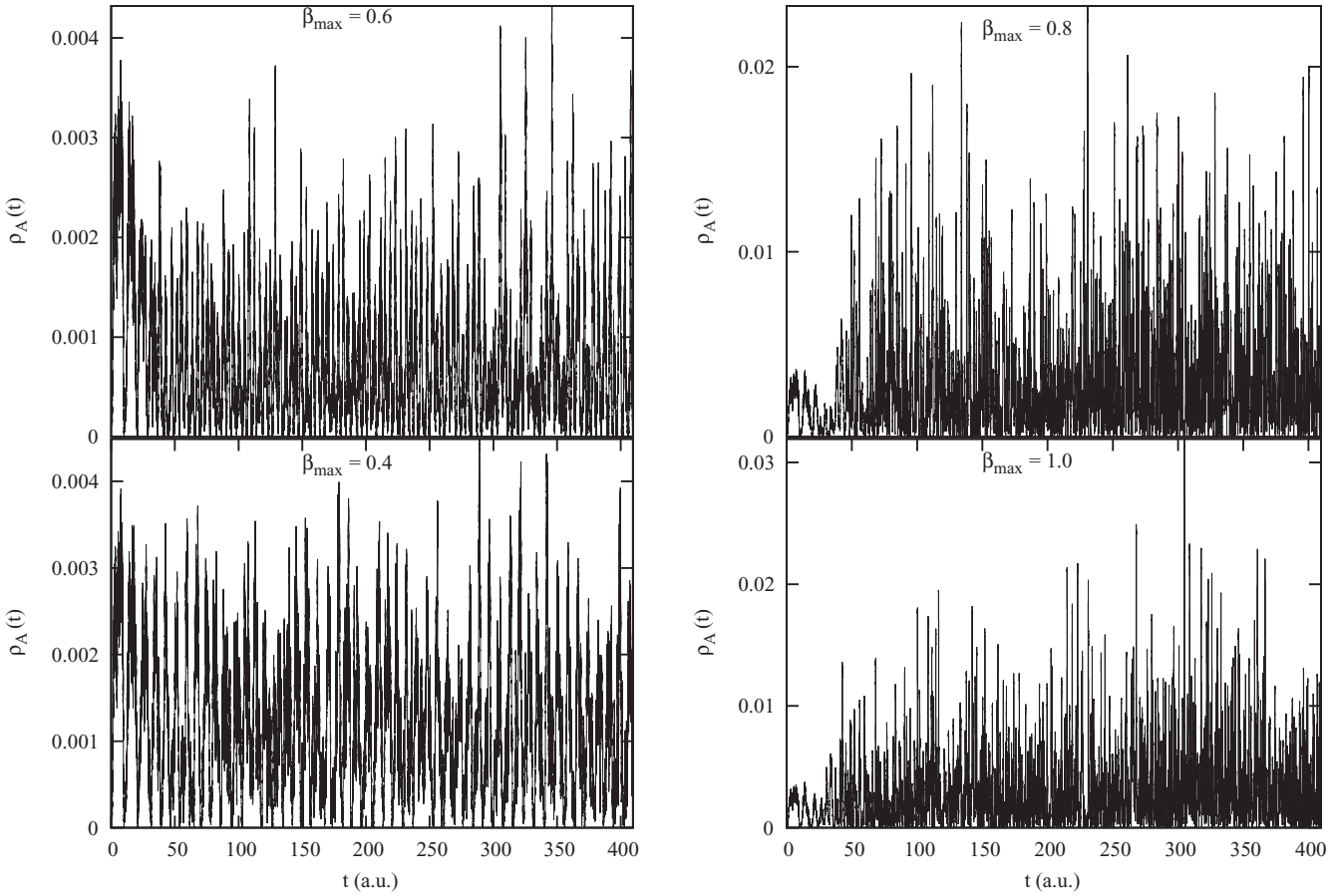

FIG. 7. Density variations (a.u.) for an observer at position A ($\tilde{\rho} = 3.0276, \tilde{z} = 0$).

The above analyses make it clear that the electron density responds in quite different ways to the TD magnetic fields depending upon $\beta_{\max}$. In a nutshell, for $\beta_{\max} \leq 0.4$ it shows an elastic behavior which tries to maintain its original configuration through the interplay between nuclear-electronic attraction and interelectronic repulsion. However, for $\beta_{\max} \geq 0.8$, the electron density cannot resist its deformation any more. Clearly, $\beta_{\max} = 0.4$ represents one extreme while $\beta_{\max} = 1.0$ represents the other. Thus, $\beta_{\max} = 0.6$ lies on the borderline where the electron density is deformed although it still tries to get back to its original configuration. Therefore, we now explore how these reorientations of density occur over time for a particular magnetic field strength.

For $\beta_{\max} = 0.4$, we have calculated the difference densities defined by Eq. (25) at the ends of 6, 8, 10, and 12 magnetic cycles (where the field vanishes); the results are depicted in Fig. 11. We began with the sixth magnetic cycle since for all cases mentioned here the dynamics which continues to the end starts by the end of the ramp, i.e., the fifth magnetic cycle. Thus, through these plots we obtain an insight into how such dynamics develops with time. On the other hand, since the dynamics has been found to retain a part of its sluggish motion when the field vanishes, we expect to see such long-time signatures in these plots. As revealed by the $\Delta\rho$ at the end of the sixth magnetic cycle, a small amount of density starts accumulating along both $\tilde{\rho}$ and $\tilde{z}$ at the cost of a depletion zone near the nucleus. At the end of the eighth magnetic cycle, this depletion zone expands due to increased interelectronic repulsions and the density primarily gets accumulated along $\tilde{\rho}$. This density accumulation increases at the end of the tenth magnetic cycle and the depletion zone advances along $\tilde{\rho}$, penetrating the positive $\Delta\rho$ region. This plot therefore indicates increased interelectronic repulsions within such density accumulation, which tries to minimize its interelectronic stresses by partial segregation along $\tilde{z}$. Such a segregation pattern has already been seen in Fig. 2. Thus, through such a spreading pattern, the electron density orients itself in small pockets along the $\tilde{z}$ direction.

In order to check whether such dynamics continues until the end of time evolution, we examine the difference densities for the aforementioned magnetic fields at the ends of 44, 46, 48, and 50 magnetic cycles in Fig. 12. At the end of the 44th magnetic cycle, one sees a small density accumulation along the $\tilde{z}$ direction instead of the $\tilde{\rho}$ direction. Along with the fact that the negative $\Delta\rho$ region is now more prominent compared to those in Fig. 11, such lateral accumulation of density implies an initiation of the "density flattening" clearly visible for higher magnetic fields. At the end of the 46th magnetic cycle, however, the density again builds up along $\tilde{\rho}$ and starts augmenting the density in the $\tilde{z}$ direction through two antennalike structures seen as a bridge between these two regions. These antennas vanish at the end of the 48th cycle where larger and denser accumulation of density is noticed in both the $\tilde{\rho}$ and $\tilde{z}$ directions. Again, due to the pressure of the

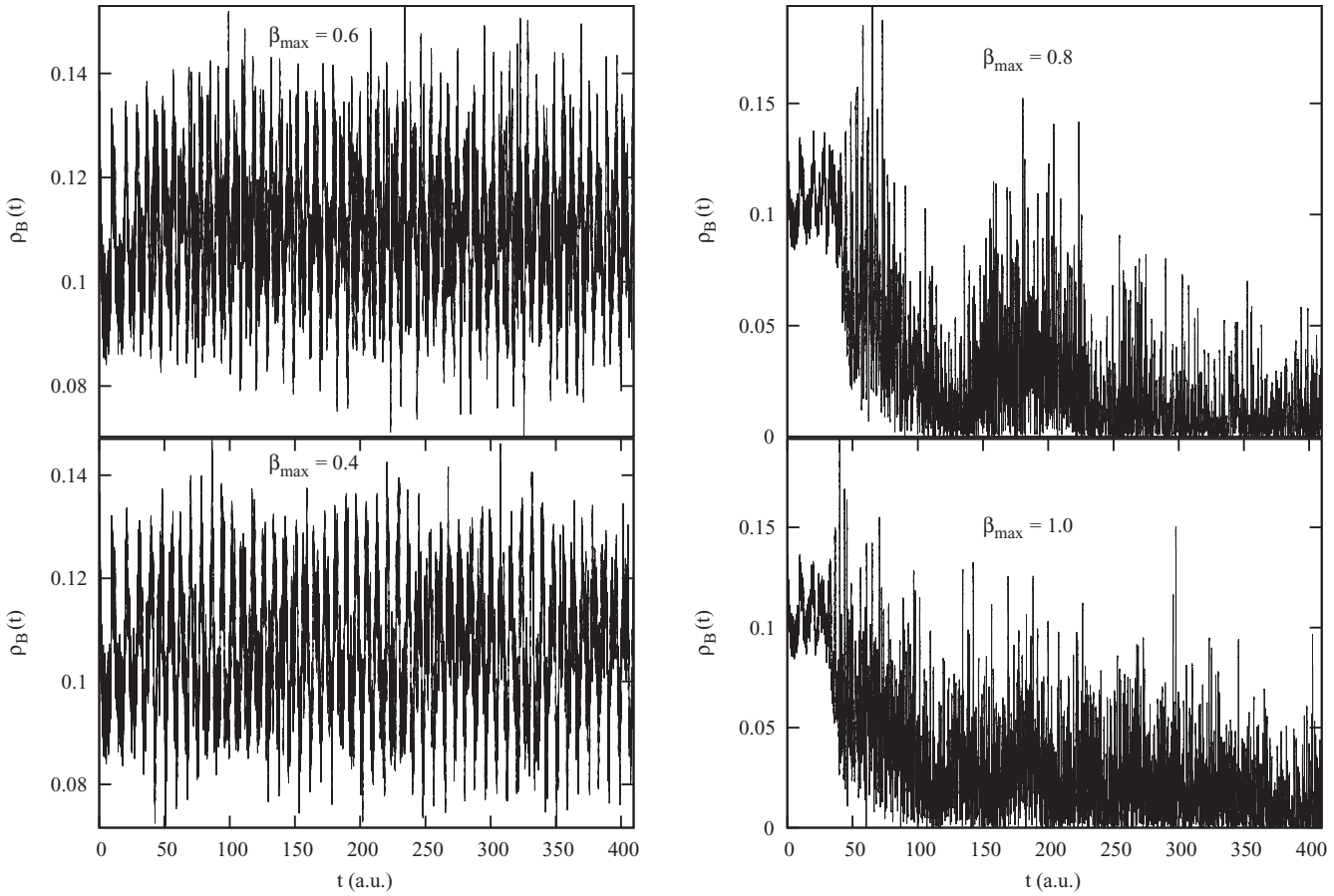

FIG. 8. Density variations (a.u.) for an observer at position B ($\tilde{\rho} = 1, \tilde{z} = 0$).

magnetic field these two positive $\Delta\rho$ regions are seen to be joined at the end of the 50th magnetic cycle, but at this time the positive $\Delta\rho$ region along $\tilde{\rho}$ shrinks because of the pressure of the magnetic field, which has been relieved by supplying density along the $\tilde{z}$ direction. Note that the negative $\Delta\rho$ region becomes more and more compact with time—an indication of increased interelectronic repulsions.

In Fig. 13, we present the difference density plots at the ends of 6, 8, 10, and 12 magnetic cycles for $\beta_{\max} = 1.0$; these plots are helpful in understanding the dynamics at the "plastic limit". At the end of the sixth magnetic cycle, one sees a compact density buildup along $\tilde{\rho}$ while the positive $\Delta\rho$ region spreads along $\tilde{z}$ at the end of the eighth magnetic cycle. Furthermore, this latter accumulation is segregated into parts, confirming large interelectronic repulsions due to high magnetic pressure. Also, note that the negative $\Delta\rho$ region has increased significantly in volume, which supports our conclusion about increased repulsive interactions. However, at the end of the tenth magnetic cycle, the density almost comes back to its original shape, leaving a small residual part leaving the $\tilde{z}$ direction, which is compensated through a large negative $\Delta\rho$ region. Thereafter, the density again starts deforming along $\tilde{z}$, leading to a significant lateral (along $\tilde{z}$) density accumulation at the end of the 12th magnetic cycle. Interestingly, there is a small region of density buildup along $\tilde{z}$ on two sides of the nucleus, which is the initiation of a new density accumulation region. Clearly, at the end of the 12th magnetic cycle the positive $\Delta\rho$ region shows a significant expansion along $\tilde{\rho}$, which is caused by the increased interelectronic repulsions that the squeezed density has to suffer due to the magnetic field.

Figure 14 depicts $\Delta\rho$ profiles for $\beta_{\max} = 1.0$ at the end of 44, 46, 48, and 50 magnetic cycles. These plots complete the picture of density motions over a range of time. As expected, we notice that at the end of the 44th magnetic cycle the electron density accumulates in pockets extending themselves along $\tilde{\rho}$ due to increased interelectronic repulsion and kinetic energy, as mentioned before. A large negative $\Delta\rho$ region is also formed, consistent with above explanations. However, the density accumulates more along $\tilde{\rho}$ at the end of the 46th magnetic cycle, making itself more vulnerable to magnetic pressure in the next magnetic cycle. Therefore, at the end of the 48th magnetic cycle we notice a number of compact, positive $\Delta\rho$ regions at lower $\tilde{\rho}$, built by the interplay of magnetic pressure and interelectronic repulsions. Such compactness, in turn, is bound to increase the interelectronic repulsions again, and at the end of the 50th magnetic cycle, the density expands again towards $\tilde{\rho}$. It is noteworthy that a small density accumulation region is visible at large $\tilde{\rho}$, which is evidence of increased pressure along $\tilde{\rho}$ creating a pocket at that point.

From the above discussions it is clear that the electron dynamics within a *single magnetic cycle* would elucidate further details of the interaction. Since one magnetic cycle contains two equivalent halves due to the sine-squared potential, we have treated the dynamics of these two halves

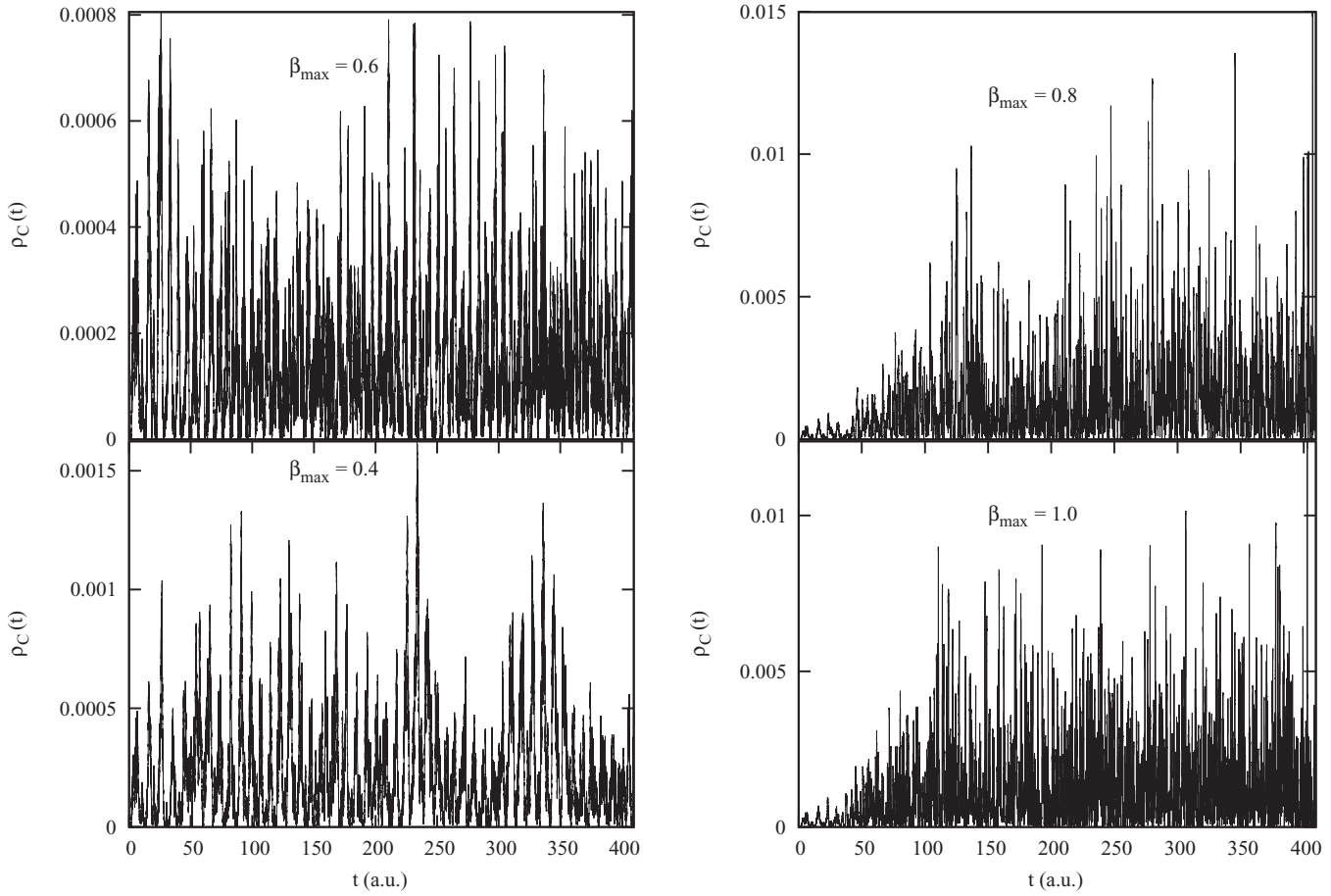

FIG. 9. Density variations (a.u.) for an observer at position C ($\tilde{\rho} = 3.0276$, $\tilde{z} = 3$).

separately and compared among themselves. For the present case we have chosen the 21st magnetic cycle for $\beta_{\max} = 0.8$ due to the fact that by this time the density is already undergoing "plastic motion" while it is still not too far from the initial state; this is helpful for comparing the phenomenon with other cases already discussed before. For this purpose, we have defined a new difference density

$$\Delta_{20}\rho(\mathbf{r},t) = \rho(\mathbf{r},t) - \rho(\mathbf{r};t = 40\pi/\omega_B), \qquad (27)$$

where $\rho(\mathbf{r};t = 40\pi/\omega_B)$ is the density after the completion of 20 magnetic cycles. Therefore, this quantity indicates how the electron density changes over one magnetic cycle with respect to the previous cycle.

For the first half of the magnetic cycle, $\Delta_{20}\rho(\mathbf{r},t)$ has been calculated with a difference of $t = \pi/4\omega_B$ and presented in Fig. 15, left-bottom panel. The first plot indicates the situation at half of the magnetic field buildup. The positive $\Delta_{20}\rho$ region indicates that as the magnetic field starts increasing density begins to move along the $\tilde{z}$ direction, although an expansion along $\tilde{\rho}$ is also visible. However, at the peak value (Fig. 15, left-top panel) the expanded electron density is pressed enough by the magnetic field to be deformed along the $\tilde{z}$ direction leading to greater interelectronic repulsion. This repulsive effect becomes operative once the magnetic field strength starts decreasing and, halfway to attaining a zero value, it again accumulates along $\tilde{\rho}$ (Fig. 15, top-right panel). Note that this accumulation still has a pattern which is similar to its previous distribution along the $\tilde{z}$ direction. Finally when the field vanishes at exactly halfway into the magnetic cycle (Fig. 15, bottom-right panel), the density starts expanding along $\tilde{\rho}$ in order to minimize interelectronic repulsions; this is also supported by the negative $\Delta_{20}\rho$ region besides the positive region near the nucleus. However, in the next half when the magnetic field again builds up, the expanded density is suppressed along $\tilde{\rho}$ (Fig. 16, left-bottom panel) which resembles the situation of the top right panel of Fig. 16, where the magnetic field strength is the same as in the present case. On the other hand, when the magnetic field again attains its peak value, the situation does not match the previous case where the magnetic field attained its peak. The density is now seen to be expanded along the $\tilde{\rho}$ axis due to interelectronic repulsions (left-top panel, Fig. 16). This feature appears to indicate that the electron density retains a memory of its previous configurations because of interelectronic repulsions. The situation of $\Delta_{20}\rho$ halfway to attaining a zero magnetic field at the end of the 21st magnetic field is depicted in the right-top panel of Fig. 16. Since the magnetic field now decreases from its peak value, the density expands along $\tilde{\rho}$, creating a depletion region near nucleus. At the end (right bottom panel, Fig. 16), when the field vanishes again, one finds a residual change in the density distribution compared to the situation of the end of the 20th magnetic cycle. As expected, this density is now extended

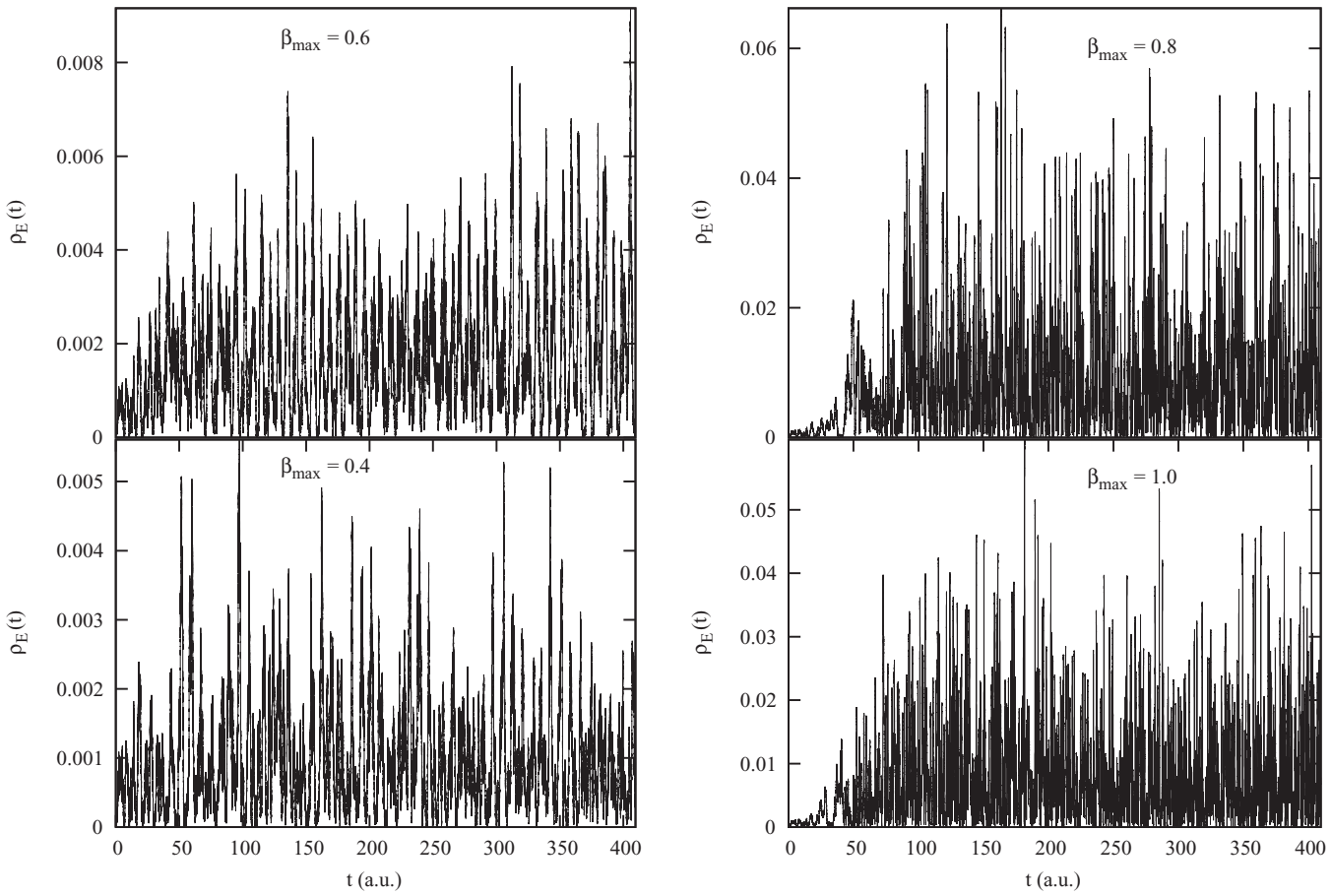

FIG. 10. Density variations (a.u.) for an observer at position D ($\tilde{\rho} = 3.0276$, $\tilde{z} = -3$).

freely towards $\tilde{\rho}$ in the absence of any magnetic pressure. This analysis confirms that even after the field vanishes the density does not come back to its initial shape and therefore retains a memory which then accumulates over a few magnetic cycles, thereby initiating a long-range dynamics.

Now, to understand how the system departs from the ground state over time as the magnetic field increases, we evaluate the autocorrelation function

$$C(t) = |\langle \Psi(t)|\Psi(0)\rangle|^2. \tag{28}$$

Clearly, if $C(t)$ remains near its $t = 0$ value of unity, the system does not deviate significantly from its ground state and the effect of the magnetic field provides simply a slight perturbation. On the contrary, for cases where $C(t)$ shows a significant decay from unity as time progresses, the system traverses more and more excited states. Figure 17 depicts the $C(t)$ plots for $\beta_{\max} = 0.2, 0.4, 0.6, 0.8$, and 1.0. For $\beta_{\max} = 0.2$, $C(t)$ remains close to 1 but oscillates with a slightly larger time period than the magnetic field, the feature observed at $\langle\tilde{\rho}\rangle(t)$ (Fig. 1) for the same magnetic field. Therefore, the emergence of a slightly slower dynamics due to the confrontation between the magnetic pressure and the interelectronic repulsions is also manifested here. It is also clear from this $C(t)$ plot that the external pressure due to the TD magnetic field is not strong enough to deform the electron density permanently and the "electron jelly" is still elastic. One can also note that just as in Fig. 1, $C(t)$ for $\beta_{\max} = 0.2$ also shows a slight bifurcation signature which is again amplified at $\beta_{\max} = 0.4$. The low-amplitude oscillation in the envelope of $C(t)$ with a longer time period confirms our previous analysis of Fig. 1. A comparison between Figs. 1 and 17 also suggests that both of these oscillations with shorter and longer time periods are opposite in phase for $\langle\tilde{\rho}\rangle(t)$ and $C(t)$, which is consistent with the above explanations.

For $\beta_{\max} = 0.6$, the $C(t)$ plot still remains close to 1 but contains more and more inner structures. It is also noted that the oscillation in the envelope is absent in this plot. While in Fig. 1 we can see a clear contraction of electron density in the $\tilde{\rho}$ direction, the present result indicates that the electron density is still trying to regain its initial structure, with partial success. However, it is clear from both Figs. 1 and 17 that during the ramp, both $\langle\tilde{\rho}\rangle(t)$ and $C(t)$ for $\beta_{\max} = 0.6$ resemble their shapes at lower magnetic fields (i.e., $\beta_{\max} = 0.2$ and 0.4), confirming that these effects gradually build up with increasing magnetic fields. On the other hand, for $\beta_{\max} = 0.8$, $C\ (t)$ drops significantly from unity near the end of the ramp (40.96 a.u.) and continues to decrease until $t \approx 50$ a.u., where it shows a small rise, but falls again until $t \approx 125$ a.u. (15th magnetic cycle). After that it shows a broad archlike structure until $t \approx 245$ a.u. (30th magnetic cycle) and continues with an oscillatory nature until the 50th magnetic cycle. However, later oscillations show smaller time periods compared with those at earlier times. Along with this oscillatory nature the envelope decays almost exponentially to zero. This decay in

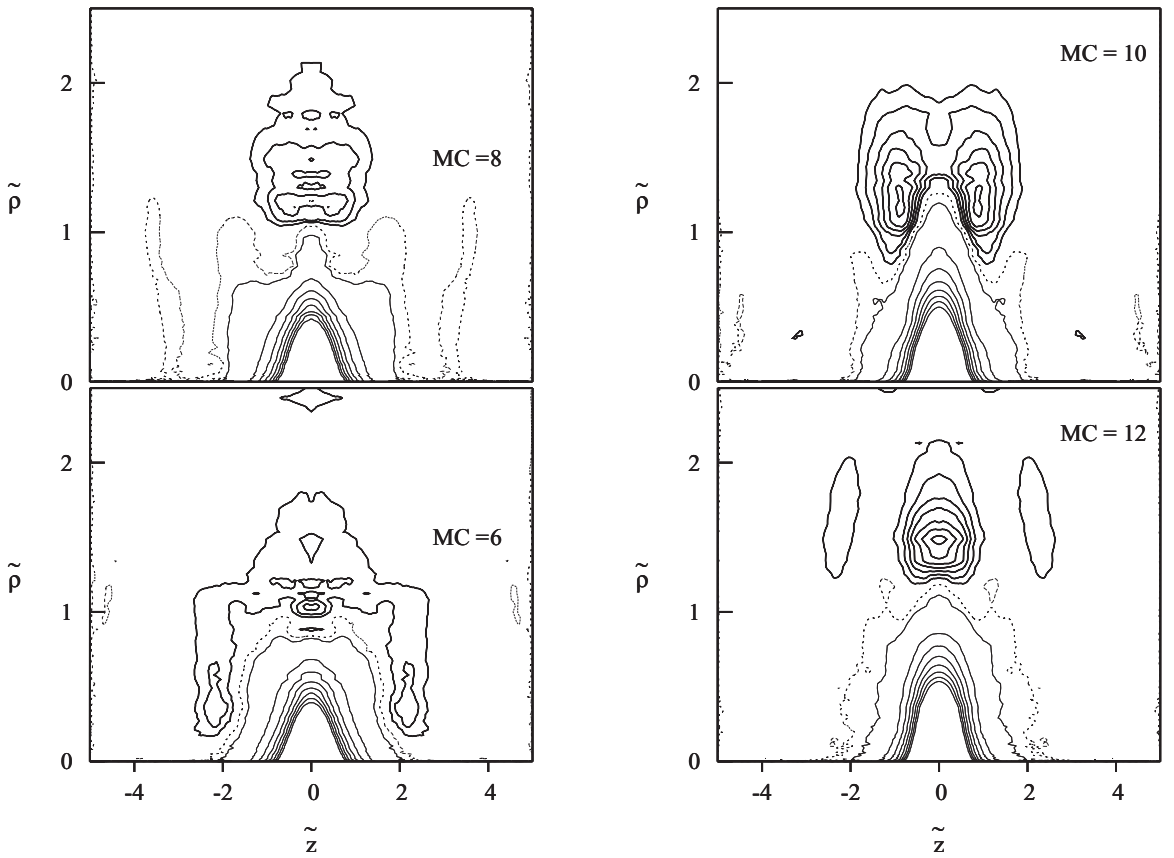

FIG. 11. Difference density ($\Delta\rho$) plots (a.u.) at the end of 6, 8, 10, and 12 magnetic cycles for $\beta_{max} = 0.4$. Note that there is no such case where the density assumes its original shape. The inner and outer contour values are the same as in Fig. 2 for both positive and negative $\Delta\rho$.

the envelope indicates that the system leaves the ground state almost entirely after some point of time while it keeps on trying to come back. This feature indicates a process of "tug of war" between two rival forces, viz., Coulomb attraction due to the nucleus, which tries to maintain a cylindrical symmetry of the electron density and the magnetic force that tries to squeeze the electron density along the $\tilde{z}$ direction. Therefore, our earlier conclusion drawn through the difference-density-based analyses is confirmed. On the other hand, for $\beta_{max} = 1.0$, the oscillating feature of $C(t)$ with a broad time period is not prominent. Nevertheless, oscillations are observed with smaller time periods. It is noteworthy that while, for $\beta_{max} = 0.8$, $C(t)$ decays to zero, for $\beta_{max} = 1.0$, $C(t)$ approaches zero only around $t \approx 350$ a.u. (42nd magnetic cycle). Thus, $C(t)$ for $\beta_{max} = 0.8$ appears to indicate a resonance energy transfer phenomenon as we reported for the H atom in TD magnetic fields [16].

In order to understand this further, we additionally investigate $C(t)$ for two intermediate magnetic fields, viz., $\beta_{max} = 0.7$ and 0.9 along with a higher magnetic field, viz., $\beta_{max} = 1.2$. Figure 18 shows these results. It can be seen that at $\beta_{max} = 0.7$ $C(t)$ indeed starts decreasing significantly from 1 but it stays near 0.4 without going down further or returning to 1. After the ramp, $C(t)$ starts showing indications of oscillation. For $\beta_{max} = 0.9$, $C(t)$ loses the broad oscillating structure of $\beta_{max} = 0.8$ by and large while still containing a resemblance of these oscillations. Moreover, $C(t)$ for $\beta_{max} = 0.9$ does not approach zero as frequently as in the $\beta_{max} = 0.8$ case. For $\beta_{max} = 1.2$, on the other hand, the oscillating nature of $C(t)$ can still be seen; it always stays above zero and rarely goes below 0.2. Based on these features one can draw two conclusions: (i) The oscillations of $C(t)$ do not depend upon its overall decay and the oscillation time periods become closer together as the magnetic field increases. (ii) As the magnetic field increases, the electron density first departs more and more from its ground state, but then with increasing magnetic fields, the extent of departure decreases. While the first conclusion implies that with higher magnetic fields the dynamics becomes more and more limited within a fewer states, transitions between them cause more harmonic variations in $C(t)$. Alternatively, one can argue that, rather than populating fewer states, more and more states stay at resonance, as in the case of the H atom. The former reason appears more plausible than the latter since the oscillation persists over a rather wide range of magnetic field strengths to be a resonance phenomenon, and the regularity builds up quite smoothly with increasing magnetic fields, which is not a characteristic feature of resonance phenomena. The second point suggests that with an increased magnetic field the electron dynamics is restricted near its ground state. This conclusion seems to be justified since the electron density is reduced near $\tilde{\rho} = 0$, and more and more density returns to the vicinity of the nucleus, with the result that the $t = 0$ state gets populated. These two explanations, taken together, imply that with increased magnetic field, a substantial part of the electron density remains close to the nucleus even for large magnetic fields. In other words, the electron density becomes "stiff"

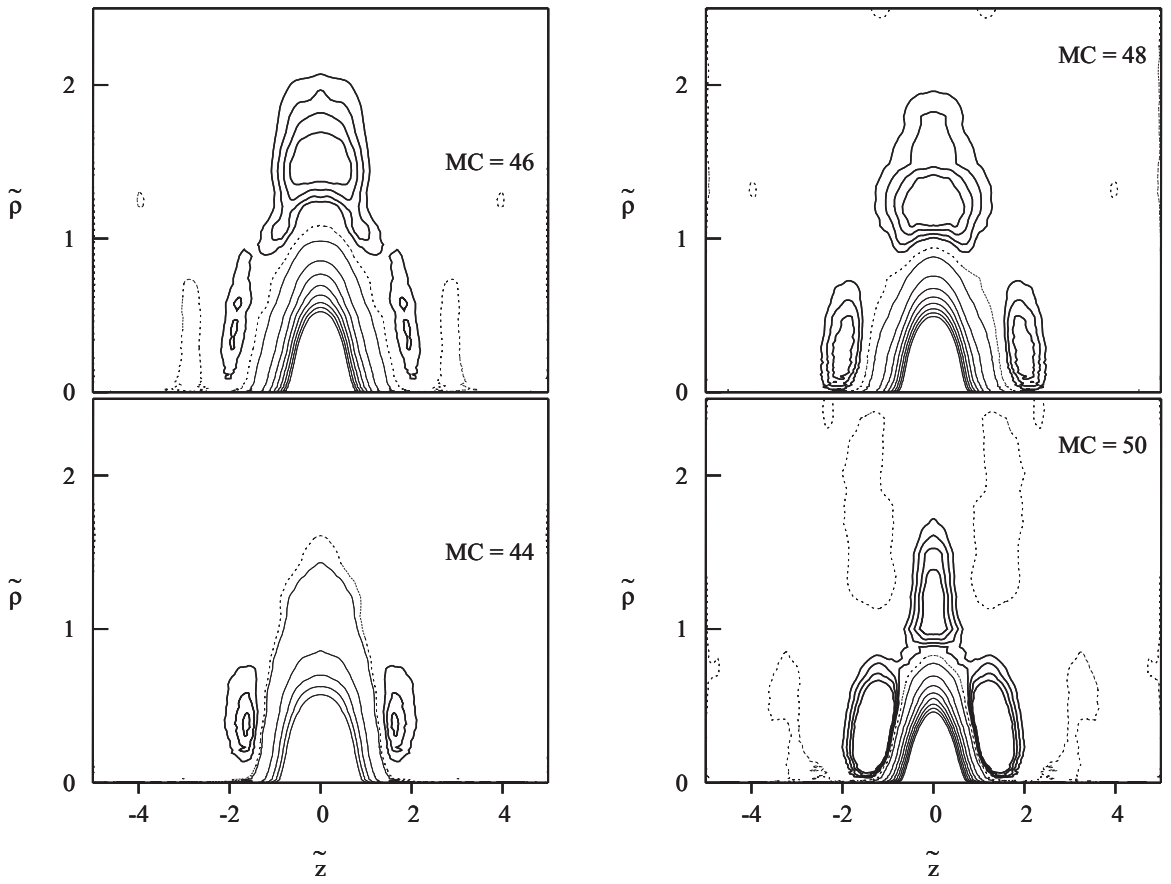

FIG. 12. Difference density ($\Delta\rho$) plots (a.u.) at the end of 44, 46, 4 and 50 magnetic cycles for $\beta_{max} = 0.4$.The inner and outer contour values are the same as in Fig. 2 for both positive and negative difference densities.

with an increase in magnetic field strength. These effects are a mixed consequence of (a) an increased nuclear attraction on the density as it returns closer to the nucleus, and (b) an available space along the $\tilde{z}$ direction which can accommodate the electron density but at the cost of diminished nuclear attraction. Clearly, electron density occupies this space since it comes out of the nuclear attraction through a confrontation between the diamagnetic force and the interelectronic repulsive force.

Therefore, we perform a fast Fourier transformation on the complex correlation function

$$\tilde{C}(t) = \langle\psi(t)|\psi(0)\rangle \tag{29}$$

for $\beta_{max} = 0.2$, 0.4, 0.6, 0.8, and 1.0, in order to obtain the power spectra

$$C(\omega) = \left| \int \tilde{C}(t) \exp(-i\omega t) dt \right|^2. \tag{30}$$

The results are shown in Fig. 19. It has been observed previously for He atom in intense laser fields that $C(\omega)$ contains peaks which match well with several excited-state energies of the atom [20,32,33]. While there is no rigorous proof yet that for all cases such signatures can be seen or that the peaks will correspond to pure states rather than dressed states, we found that for $\beta_{max} = 0.2$, 0.4, and 0.6 we do not see more than a single peak with no peak at $\omega \geq 0$. For $\beta_{max} = 0.2$, the peak position is at $\omega = -0.8868$ a.u., which shifts to $\omega = -0.8149$ a.u. for $\beta_{max} = 0.4$ and to $\omega = -0.7191$ a.u. for $\beta_{max} = 0.6$. It is observed that the energies of the ^1S ($1s2s$) and $^1P^0$ ($1s2p$) states have energies -0.8384 a.u. and -0.8629 a.u., respectively, while there is no state which has energy near -0.7191 a.u. Thus, the peaks at $\beta_{max} = 0.4$ and 0.6 are relatively shifted from the $^1P^0$ and ^1S states by almost the same amount, i.e., 0.024 a.u. Clearly, for $\beta_{max} = 0.2$, the density contains a significant contribution from the $1s2p$ configuration while at $\beta_{max} = 0.4$ the dominant contribution is from $1s2s$. However, for $\beta_{max} = 0.6$, the peak corresponds to a dressed state. Since compared to the $\beta_{max} = 0.2$ case the density is more squeezed towards the nucleus at $\beta_{max} = 0.4$, the electron density occupies the $1s2s$ configuration which is more compact than $1s2p$. The increased effect of magnetic fields at $\beta_{max} = 0.6$, therefore, changes the system itself to a quite different system such that the major contribution now arises from a dressed state rather than a shifted atomic state of the He atom. For $\beta_{max} = 0.8$, one sees that the single peak is now split into ten distinct peaks. The peak positions are recorded at -0.5512 a.u. (a), -0.8149 a.u. (b), -0.9827 a.u. (c), -1.0306 a.u. (d), -1.1025 a.u. (e), -1.1504 a.u. (f), -1.2464, a.u. (g), -1.3183 a.u. (h), -1.3902 a.u. (i), and -1.4381 a.u. (j). Among them, peaks (b) and (c) represent $1s2p$ ($^1P^0$) and $1s4s$ (^3S) states, again shifted by -0.0239 a.u. The other peaks do not match any other unperturbed state of He. For $\beta_{max} = 1.0$, again ten peaks appear with energies -0.7669 a.u. (a), -0.8149 a.u. (b), -0.9827 a.u. (c), -1.1025a.u. (d), -1.1744 a.u. (e), -1.2463 a.u. (f), -1.2943 a.u. (g), -1.3662 a.u. (h), -1.4141a.u. (i),

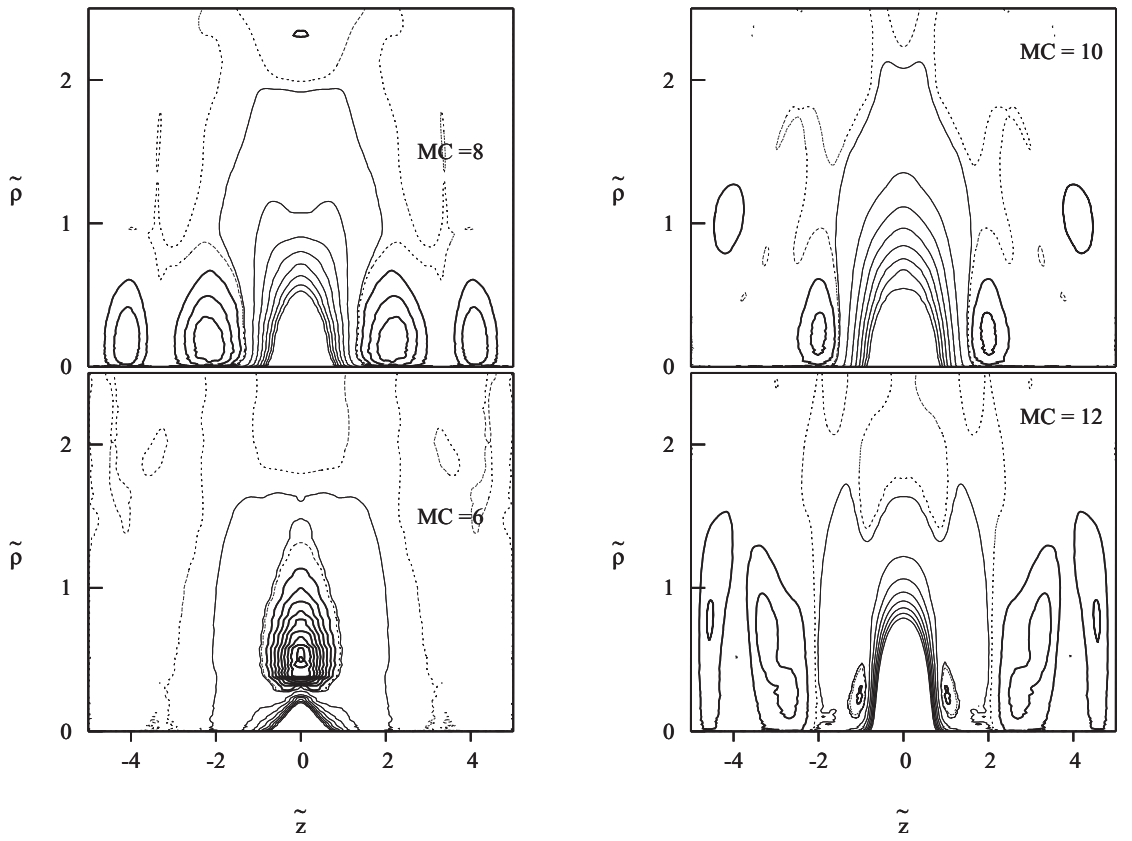

FIG. 13. Difference density ($\Delta\rho$) plots (a.u.) at the end of 6, 8, 10, and 12 magnetic cycles for $\beta_{\max} = 1.0$. Note the positive $\Delta\rho$ pocket as a consequence of electronic repulsions. The inner and outer contour values are the same as in Fig. 2 for both positive and negative $\Delta\rho$.

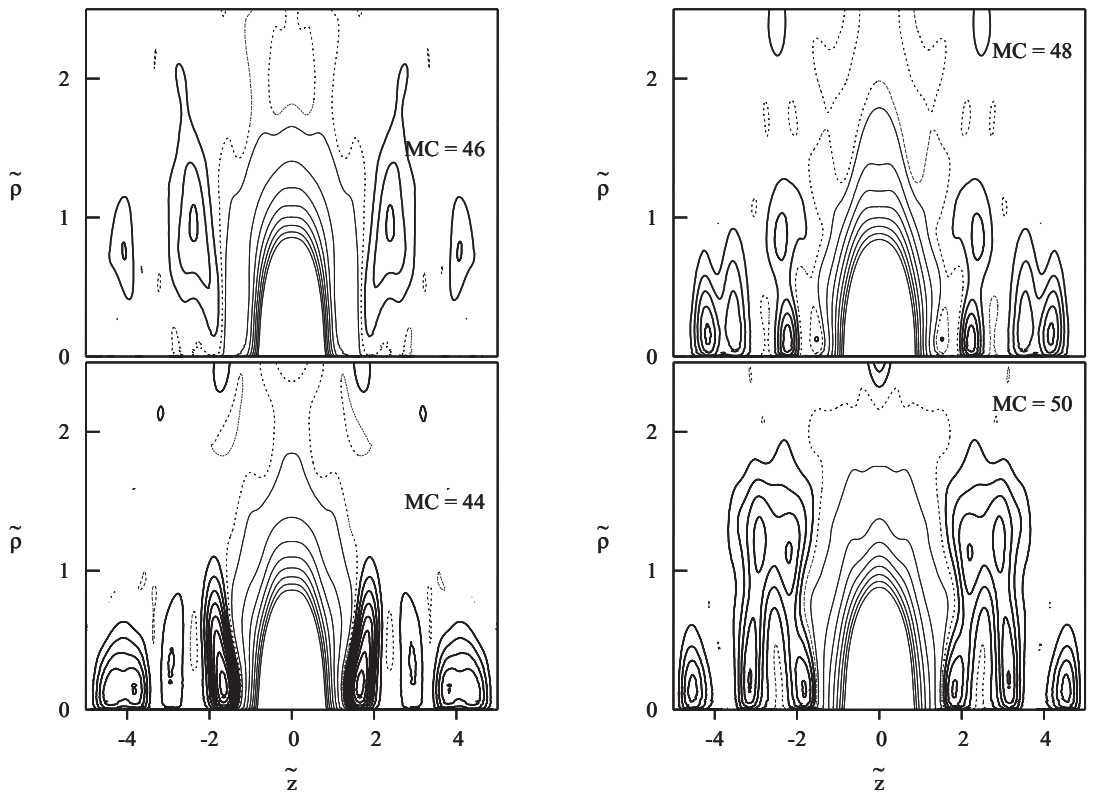

FIG. 14. Difference density ($\Delta\rho$) plots (a.u.) at the end of 44, 46, 48, and 50 magnetic cycles for $\beta_{\max} = 1.0$. The number of positive difference density pockets has increased, showing their own dynamics.

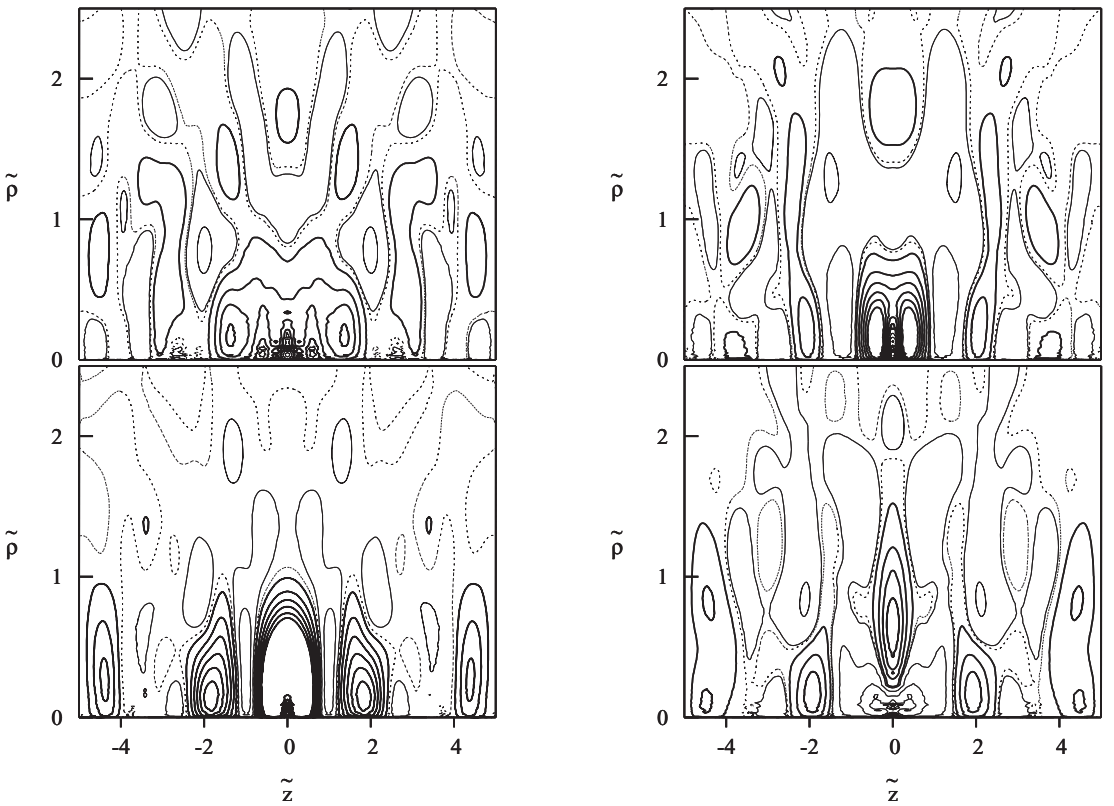

FIG. 15. The difference density ($\Delta_{20}\rho$), defined by Eq. (27) in a.u., at the 21st magnetic cycle for $\beta_{\max} = 0.8$. The sequence of snapshots is from bottom left clockwise to bottom right, where the field vanishes.

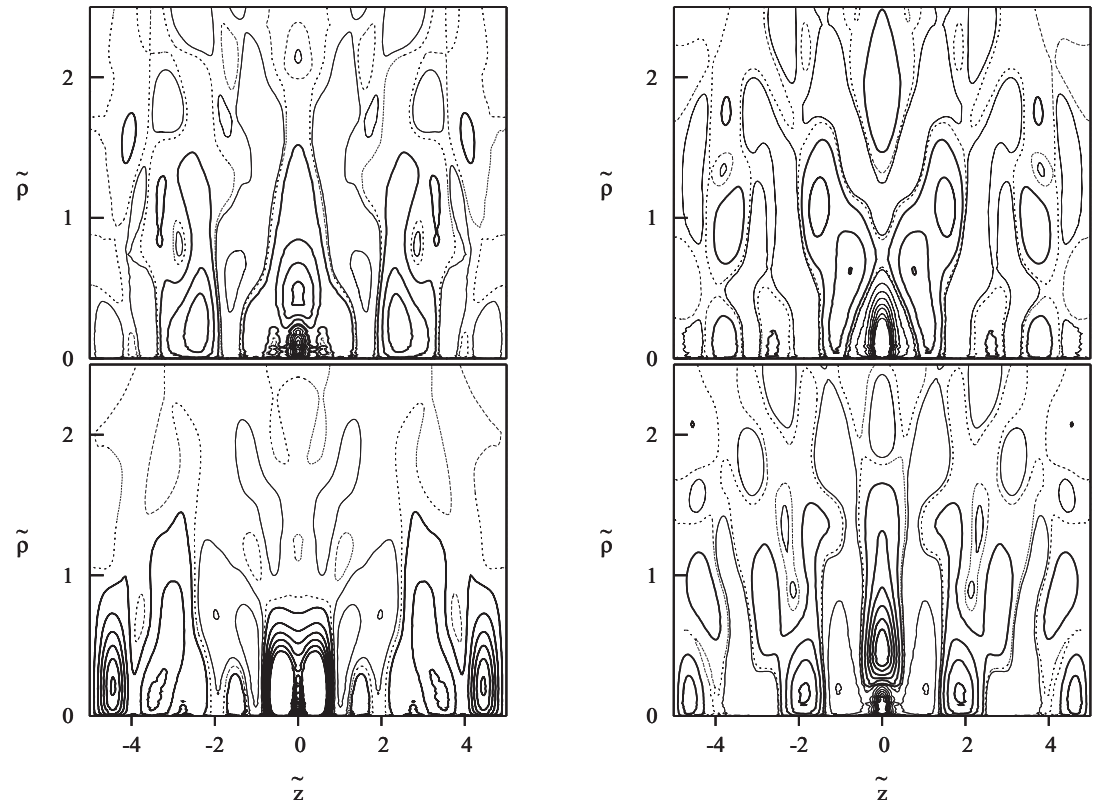

FIG. 16. The same quantity (a.u.) as in Fig. 15 for the next half of the 21st magnetic cycle for $\beta_{\max} = 0.8$. The sequence is identical to that in Fig. 15.

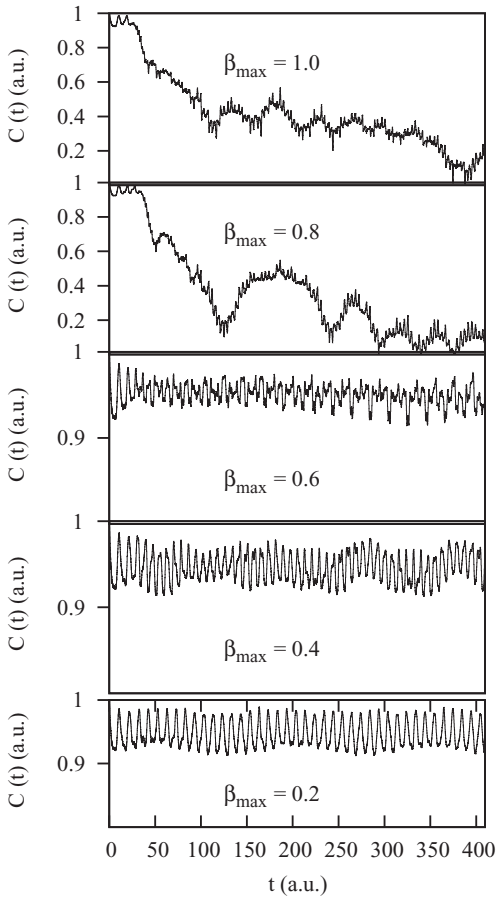

FIG. 17. The autocorrelation function $C(t)$, defined in a.u. by Eq. (28) for $\beta_{\max} = 0.2$, 0.4, 0.6, 0.8, and 1.0 from bottom to top. Notice the change of structure, from $\beta_{\max} = 0.6$ to $\beta_{\max} = 0.8$, as in Fig. 1.

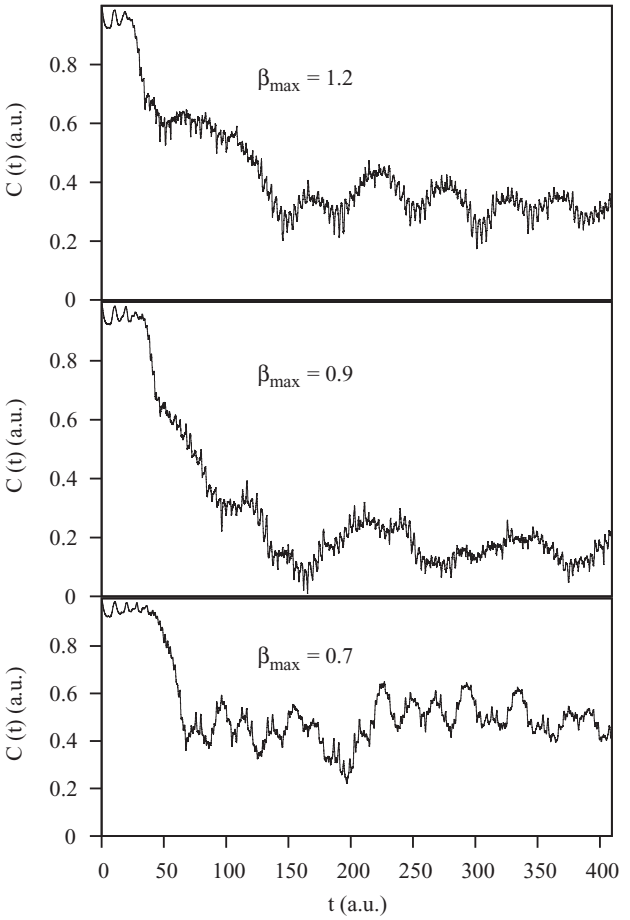

FIG. 18. $C(t)$ plots (a.u.) for $\beta_{\max} = 0.7$, 0.9, and 1.2. The gradual changes in features are now seen clearly and hence these plots bridge the transition noted in Fig. 17 (see text).

and -1.4620 a.u. (j). We can again identify (b) and (c) as $1s2p$ and $1s4s$ states, while others remain unidentified and correspond to dressed states. However, it is observed that the (a) peaks of these two cases, are shifted from each other by -0.2157 a.u. while there is no shift for (b) and (c), a shift of -0.959 a.u. for (d), a common -0.0479 a.u. shift for (e) and (f), and a common -0.0239 a.u. shift for (g) and (h) for the two magnetic fields concerned. Further investigations are required to understand such shifts.

All the above discussions assumed the $\tilde{z}$ parity of the electron density throughout. Consequently, throughout the time evolution no significant electrical dipole moment (a measure of $\tilde{z}$ asymmetry) should be seen. For all the cases dealt with in this paper, the electric dipole moments are seen to be $\sim 10^{-3}$ and fluctuate randomly over time around zero. Although the magnitudes of such fluctuations increase from 10^{-5} upwards with increasing magnitudes of the magnetic fields, we attribute these fluctuations to numerical inaccuracies rather than a physical phenomenon for the following reasons:

With an increase in magnetic field strength, numerical errors occur near grid boundaries since the magnetic field spreads the electron density in the $\tilde{z}$ direction. A small error δ in the density at a single point near a grid boundary causes an electric dipole moment of δ multiplied by the distances between the two $\tilde{z}$ boundaries, i.e., 10δ in the present case. Due to our quadratically scaled $\tilde{\rho}$ axis, most of the $\tilde{z}$ boundary grid points are close to the nucleus, which might magnify the errors. With an increase of $\beta_{\max}$, more and more density accumulates near the nucleus, which increases this dipole moment further. However, had the electric dipole moment been a physical phenomenon it would not show a random time structure which does not follow the magnetic field time structure at all. Moreover, in the presence of such a physical electric dipole moment, the presence of $m \neq 0$ states in the time-evolved density cannot be ruled out, which would nullify our analyses in the previous section, and the DC equation in this present form itself would not be valid. In view of the internal consistency of our analysis we can conclude that the $\tilde{z}$ parity of the system is retained over the entire time evolution.

IV. CONCLUSION

In the present work, we have demonstrated that the electron density of a He atom interacting with strong, oscillating magnetic fields responds through a sluggish dynamics. Sluggish dynamics was also observed in the case of the H atom [16]. In the case of the H atom, the electron dynamics was a consequence of a confrontation between the nuclear field and the magnetic field. However, in the case of the He

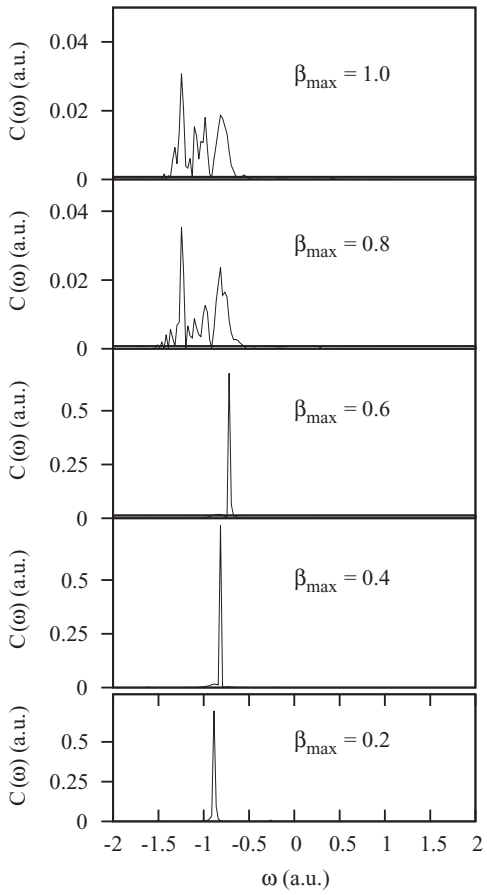

FIG. 19. $C(\omega)$ plots (a.u.) corresponding to the $C(t)$ plots of Fig. 17. These plots also show a paradigm shift above $\beta_{max} = 0.6$ (see text).

atom, the presence of an additional electron ensures that such dynamics occurs due to a triangular confrontation between interelectronic repulsions, the nuclear field, and the magnetic field, leading to rich features in the density variations as discussed in detail in the text. In particular, this triangular confrontation leads to a spread in the electron density along a direction perpendicular to that of the magnetic field. At first sight, this might appear counterintuitive, but actually it is not. Second, unlike for the H atom, there is now a threshold value of the magnetic field for the electron density to change over smoothly from an "elastic flow" to a "plastic flow" at higher magnetic fields. This is because, as we observe in this work, under strong, TD magnetic fields the electron density behaves either like an "elastic" or a "plastic ball of jelly" depending upon the magnetic field strength.

The interelectronic repulsions' (a combination of Coulomb, exchange, and correlation terms) nonlinear dependence on the magnetic field strength plays a significant role in deciding where in space the electron density should be augmented and where it should be depleted. Such density distributions tend to minimize interelectronic stresses. In particular, the TD correlation "energy", a significant part of the interelectronic repulsions, decreases at higher magnetic fields as the electron density begins its plastic flow. Interestingly, at higher magnetic fields, the electron density responds differently to the two halves of a magnetic cycle, leading to prominent bifurcations in the density oscillations. Note that the interelectronic repulsion terms' dependence on the magnetic field strength occurs through their dependence on the electron density which itself depends on the magnetic field. Needless to say, the present strong-field results cannot be explained by a perturbative approach in which the perturbation is much smaller compared to the unperturbed Hamiltonian.

Although, in the present study, we did not find any indication of ionization due to magnetic fields, further studies on different atoms or molecules under wider ranges of magnetic field strengths would be of interest. While we did not study the effects of the magnetic field frequencies on the dynamics, such studies should also form a subject of future interest. The present study also suggests that, for certain parameters, a resonance-type phenomenon may be operative between the He atom and the magnetic fields, as occurs with the H atom [16]. A detailed identification of unperturbed, Zeeman-shifted, and dressed states would help to provide more insights into the nature of such interactions.

Finally, it is worthwhile to note that a completely general treatment of the present TD problem, valid for all states of known space-spin symmetries, in terms of either the many-electron TD wave function or the two-electron TD reduced density matrix, would be very complicated and may no longer remain transparent to physical interpretation, unlike the present treatment. Additionally, the density matrix would suffer from the intractable N-representability problem besides severe computational difficulties. The density-functional approach, as described in the present work, offers a simple, accurate and physically transparent alternative.

ACKNOWLEDGMENTS

We gratefully acknowledge IISER-Kolkata for providing computer facilities. M.S. thanks the C.S.I.R., New Delhi, for a Senior Research Fellowship. B.M.D. thanks the Indian National Science Academy, New Delhi, for financial support and Professor Sushanta Dattagupta for hospitality, first at IISER-Kolkata and then at Visva-Bharati University.

[1] Y. Yafet, R. W. Keys, and E. N. Adams, J. Phys. Chem. Solids **1**, 137 (1956).
[2] R. J. Elliot and R. Louden, J. Phys. Chem. Solids **15**, 196 (1960).
[3] J. Trümper, W. Pietsch, C. Reppin, W. Voges, R. Staubeit, and E. Keudziorra, Astrophys. J. **219**, L105 (1978).
[4] Los Alamos National Laboratory http://www.lanl.gov/orgs/mpa/nhmfl/
[5] G. Thurner, H. Körbel, M. Braun, H. Herold, H. Ruder, and A. K. Rajagopal, Phys. Rev. D **9**, 329 (1974).
[6] M. D. Jones, G. Ortiz, and D. M. Ceperley, Phys. Rev. A **54**, 219 (1996).

[7] O.-A. Al-Hujaj and P. Schmelcher, Phys. Rev. A **68**, 053403 (2003).
[8] W. Becken and P. Schmelcher, Phys. Rev. A **63**, 053412 (2001).
[9] W. Becken and P. Schmelcher, Phys. Rev. A **65**, 033416(2002).
[10] M. D. Jones, G. Ortiz, and D. M. Ceperley, Int. J. Quantum Chem. **64**, 523 (1997).
[11] M. D. Jones, G. Ortiz, and D. M. Ceperley, Phys. Rev. E **55**, 6202 (1997).
[12] M. Braun, Phys. Rev. A **65**, 033415 (2002).
[13] Z. Medin and D. Lai, Phys. Rev. A **74**, 062507 (2006).
[14] D. Neuhauser, S. E. Koonin, and K. Langanke, Phys. Rev. A **36**, 4163 (1987).
[15] D. Lai, Rev. Mod. Phys. **73**, 629 (2001); M. Sadhukhan and B. M. Deb, in *Theoretical and Computational Developments in Modern Density Functional Theory*, edited by A. K. Roy (Nova Science, New York, 2012).
[16] M. Sadhukhan, P. K. Panigrahi, and B. M. Deb, Europhys. Lett. **91**, 23001 (2010).
[17] M. Sadhukhan and B. M. Deb, Europhys. Lett. **94**, 50008 (2011).
[18] K. C. Kulander, Phys. Rev. A **36**, 2726 (1987).
[19] R. V. Jensen and B. Sundaram, Phys. Rev. Lett. **65**, 1964 (1990).
[20] B. K. Dey and B. M. Deb, Int. J. Quantum Chem. **56**, 707 (1995).
[21] B. K. Dey and B. M. Deb, Int. J. Quantum Chem. **70**, 441 (1998).
[22] X. Guan, X.-M. Tong, and S.-I. Chu, Phys. Rev. A **73**, 023403 (2006).
[23] B. M. Deb and P. K. Chattaraj, Phys. Rev. A **39**, 1696 (1989).
[24] B. M. Deb and S. K. Ghosh, J. Chem. Phys. **77**, 342 (1982); E. Runge and E. K. U. Gross, Phys. Rev. Lett. **52**, 997 (1984).
[25] A. Wadehra and B. M. Deb, Eur. Phys. J. D **39**, 141 (2006).
[26] S. K. Ghosh and A. K. Dhara, Phys. Rev. A **38**, 1149 (1988).
[27] M. Sadhukhan and B. M. Deb, J. Mol. Struct.:THEOCHEM **943**, 65 (2010).
[28] B. M. Deb and P. K. Chattaraj, J. Sci. Ind. Res. **43**, 238 (1984).
[29] A. K. Roy, B. K. Dey, and B. M. Deb, Chem. Phys. Lett. **308**, 523 (1999).
[30] R. Singh and B. M. Deb, Phys. Rep. **311**, 47 (1999).
[31] E. Clementi and C. Roetti, At. Data Nucl. Data Tables **14**, 174 (1974).
[32] R. G. Parr and W. Yang, *Density Functional Theory of Atoms and Molecules* (Oxford University Press, Oxford, 1994), p. 55.
[33] C. E. Moore, *Atomic Energy Levels*, Natl. Bur. Stand. (U.S.) Circ. No. 467 (U.S. GPO, Washington, D.C., 1949), pp. 4–7.